Runx2 links the DNA damage response to osteogenic reprogramming and apoptosis of vascular smooth muscle cells

Andrew M. Cobb[1], Syabira Yusoff[1], Robert Hayward[1], Sadia Ahmad[1], Mengxi Sun[1], Anja Verhulst[2], Patrick C. D'Haese[2] and Catherine M. Shanahan[1]*

[1]*BHF Centre of Research Excellence, School of Cardiovascular Medicine and Sciences, King's College London, The James Black Centre, 125 Coldharbour Lane, London SE5 9NU, United Kingdom.*
[2]*Laboratory of Pathophysiology, Department of Biomedical Sciences, University of Antwerp, Universiteitsplein 1, 2610 Wilrijk, Belgium*

Short title: DNA damage drives calcification via Runx2

*To whom correspondence should be addressed:

Corresponding Author:
Professor Catherine Shanahan
James Black Centre
125 Coldharbour Land
London SE5 8NU, UK

Tel.: 44 20 7848 5221
Fax: 44 20 7848 5193
e-mail: cathy.shanahan@kcl.ac.uk

Word count: 11,010

Abstract

Objective: The development of ectopic vascular calcification is strongly linked with organismal ageing, which is primarily caused by the accumulation of DNA damage over time. As Runx2 has been identified as a regulator of vascular smooth muscle cell (VSMC) osteogenic transition, a key component of vascular calcification, we examined the relationship between DNA damage and Runx2 activation.
Approach and results: We found genotoxic stress stimulated Runx2 accumulation and transactivation of its osteogenic target genes, leading to enhanced calcification. Inhibition of DNA damage signalling attenuated this response. Runx2 localized to sites of DNA damage and participated in DNA repair by regulating phosphorylation events on histone H2AX, with exogenous expression of Runx2 resulting in unrepaired DNA damage and increased apoptosis. Mechanistically, Runx2 was PARylated in response to genotoxic stress and inhibition of this modification disrupted its localisation at DNA lesions and reduced its binding to osteogenic gene promoters.
Conclusions: These data identify Runx2 as a novel component of the DNA damage response, coupling DNA damage signalling to both osteogenic gene transcription and apoptosis and providing a mechanism for accelerated mineralisation in ageing and chronic disease.

Key words: Runx2 / Vascular calcification / DNA damage / PARylation / Ageing

Non-standard abbreviations used in this study

Phosphorylated serine 139 on H2AX	γH2AX
Phosphorylated tyrosine 142 on H2AX	pY142-H2AX
Recombinant Flag-tag Runx2	FL-Runx2
Short hairpin RNA against Runx2	shRunx2
Boronate bead pull-down assay	BBPDA

Introduction

Ectopic vascular calcification invariably increases with age and is a major risk factor for cardiovascular mortality. [1 2, 3] It is a cell-mediated process driven by vascular smooth muscle cells (VSMCs) [4, 5] that ordinarily are essential for maintaining vascular tone through their contractile activity. However, in ageing and disease these cells display marked phenotypic plasticity and can undergo osteochondrogenic differentiation. This transition is characterised by a loss of contractile markers [6] and increased expression of osteogenic factors including the master transcription factor Runt-related transcription factor 2 (Runx2) and its downstream osteogenic targets Osterix, [7] Osteocalcin (OCN) [8] and Bone sialoprotein (BSP). [9-11] Increased secretion of calcifying vesicles [12] and a higher incidence of apoptosis [13, 14] are also recognised features of this osteogenic switch which orchestrates the calcification process. However, the specific pathways that link these processes with ageing have remained elusive.

Runx2 is essential for developmental osteogenesis in bone [15, 16], but it has functions beyond activation of osteogenic transcriptional programmes and is expressed in a number of non-mineralizing cell types. [17] In the vasculature, Runx2 is upregulated at sites of calcification and targeted knockout of Runx2 reduces expression of its osteogenic targets and reduces calcification. [18-21] Notably, however, Runx2 is transiently upregulated in the absence of calcification at sites of vascular injury [22] while targeted over-expression of Runx2 in VSMCs *in vivo* is insufficient for calcification to ensue [23] suggesting that additional factors or modifications are required to activate its osteogenic capacity.

Runx2 acts as a scaffold to organise enhancers and repressors and its transcriptional activity is dependent on its localisation to the nuclear matrix. [24, 25] This proteinaceous network acts to organise nuclear metabolic events, including transcription and the DNA damage response (DDR) [26-28] and emerging evidence suggests that Runx2 may have a direct function in the DDR [24, 29], with its deregulation in a range of cancers further substantiating this notion. [30-32] Importantly, DDR regulators are also instrumental during normal physiological bone formation and in ectopic vascular calcification [33-35] suggesting a link between Runx2 activity, DNA damage repair and osteogenesis.

A primary event in the DDR is phosphorylation of histone H2AX on serine 139 (γH2AX) by the kinase Ataxia-telangiectasia mutated (ATM) [36] and cells positive for γH2AX are detectable in the bone growth plate and in calcified arteries. [35] In addition, ATM and DDR effector proteins c-Abl, and p53 have been shown to regulate osteoblast activity. [37, 38] Another key DDR component is Poly(ADP-ribose) (PAR) polymerase (PARP) signalling. This pathway, usually activated by oxidative stress, involves the post-translational addition of PAR moieties - by PARP enzymes - to target proteins in a process termed PARylation. PARP1 has been shown to play a role in osteogenic differentiation in bone [39] and high levels of PAR have been detected in the bone growth plate and at sites of vascular calcification. [35, 40, 41] PAR itself can avidly bind calcium and form calcified nanoparticles, suggesting a by-product of the DDR is also essential for biomineralization. [35] Inhibitors of DDR signalling can block osteogenic differentiation and calcification in both bone and the vasculature, however the mechanisms behind this remain unclear. [33, 35]

In this study we hypothesised that DDR signalling might activate Runx2-mediated osteogenesis in the vasculature. Using *in vitro* and *in vivo* models of Runx2 depletion and over-expression we show that Runx2 is a novel component of the DDR that regulates H2AX phosphorylation in response to DNA damage and promotes apoptosis. PARylation of Runx2 was essential for this activity and for its activation of osteogenic gene expression in VSMCs. This is the first time a precise role for Runx2 during the DDR has been reported and our data

provides an explanation for the increased incidence of vascular calcification observed with age and highlights the potential for DDR inhibitors as therapeutics for vascular calcification.

Materials and methods

The authors declare that all supporting data are available within the article [and its online supplementary files].

Cell culture / treatments - VSMCs were obtained from explants of human aortic tissues from both male and female donors of various ages as previously described. [42] The isolates used in this study were as follows; 35F (04:35F:11A), 20M (05:20M:18A) and 54M (05:54M:20). Cells were maintained in M199 medium (Sigma Aldrich) supplemented with 20 % fetal bovine serum (FBS) at 37 °C and 5 % CO_2 and used between passages 9 and 20. Control mouse VSMCs (*Runx2*$^{f/f}$) and Runx2 KO VSMCs (*Runx2*$^{\Delta SM}$) were cultured in the same media. To induce calcification, VSMCs were cultured in M199 medium supplemented with 5 % FBS and elevated calcium (Ca^{2+}) and phosphate (P_i) (2.7 mM and 2.5 mM respectively) for between 8-15 days until signs of calcification became apparent. Control medium was M199 with 5 % FBS and no additional Ca^{2+} or P_i (1.8 mM and 1 mM respectively). For short-term DNA damage induction, cells were typically treated for 0.5 - 3 hours with 20 μM etoposide or 200 mM H_2O_2. For long term treatments performed alongside calcification experiments (>24 hours) concentrations of 5 μM etoposide or 20 mM H_2O_2 were used. Inhibitors against PARP, ATM and mitogen-activated protein kinase (MEK), (PJ34 (AdipoGen), KU55933 (Selleckchem), U0126 (Sigma Aldrich) respectively) were used at 10 μM. DMSO was used as a vehicle control.

Generation of conditional Runx2 KO mice - The conditional Runx2 Knock-Out (KO) mouse model was generated by Taconic-Artemis. The targeting strategy was based on the Ensembl transcript ENSMUST00000160673 (Runx2-001) which allows conditional KO of the Runx2 gene (*Runx2*). The *Runx2* targeting vector was created by flanking the *Runx2* targeted domain of exon 4 with *loxP* sites and the positive selection marker Puromycin-resistant (PuroR) was flanked by FRT sites. The targeting vector was generated using bacterial artificial chromosome (BAC) clones from C56LB/6J RPCIB-731 BAC library. The target vector was injected into embryonic stem cells from Taconic Artemis C57BL/6N by electroporation and cells with successful homologous recombination were isolated using positive (PuroR) and negative (Thymidine Kinase-Tk) selections. These were injected into C57BL/6 mouse blastocysts to generate chimeric floxed-Runx2 mice which were then bred onto a FLP recombinase strain to remove the Puromycin cassette. To generate smooth muscle cell (SMC)-specific Runx2 KO mice (*Runx2*$^{\Delta SM}$*), Runx2*$^{f/f}$ mice were crossed with mice expressing SMC-specific Cre recombinase which is driven by the SM22-α promoter. The SM22 Tg(Tagln-cre)1Her/J mice (004746; The Jackson Laboratory). Genotyping was performed using PCR of DNA extracted from ear biopsy specimens. Primers used for genotyping were as follows: Runx2 conditional KO; forward 5' GAGCTAGCCTAGCCTTTCTGC 3' and reverse 5' CAAGAGGACTCAAGTTCAGATCC 3'. Cre recombinase expression; forward 5' GCGGTCTGGCAGTAAAAACTATC 3' and reverse 5'GTGAAACAGCATTGCTGTCACTT 3'. Cycling parameters were the following: initial denaturation 95°C, 5 minute; denaturation 95 °C ,30 seconds (repeated for 35 cycles); annealing 60 °C, 30 seconds (repeated for 35 cycles); extension 72 °C, 1 minute (repeated for 35 cycles); final extension 72 °C, 10 mins; cooled to 4°C indefinitely. The PCRs produced amplicons of 197bp (wild-type allele) 354bp (Conditional KO allele) and 100bp (Cre recombinase). *Runx2*$^{f/f}$ and *Runx2*$^{\Delta SM}$ mice were maintained on a C57BL/6 background. All

mice were kept in individually ventilated cages at the biological services unit at the Maurice Wohl Clinical Neuroscience Institute, King's College London. They were maintained on a normal diet (LabDiet 5053 / PicoLab Rodent Diet 20) and kept on a 12-hour light/dark cycle. Male and female mice were used in this study. All experiments were carried out in accordance with the UK Animal (Scientific Procedures) Act 1986 and were covered by a Home Office project licence.

Vitamin D induction of calcification in mice - Vitamin D treatment is an established model used to induce vascular calcification in mice. It causes dysregulation of calcium metabolism, resulting in increased serum calcium but unchanged phosphate levels.[43] For this treatment, Cholecalciferol (C1357; Sigma) was dissolved in 100 % ethanol and diluted to 1.25 µg/µl containing 5 % ethanol for each injection. Twenty-week-old *Runx2$^{f/f}$* and *Runx2$^{\Delta SM}$* mice on a C57BL/6 background received cholecalciferol subcutaneously at a dosage of 500,000 IU/kg/day for 4 consecutive days, and 5 % ethanol in sterile water was used as vehicle control. [18] The mice were monitored daily and terminated between 7 to 8 days after injection. Thoracic aortas were collected for calcium quantification, RNA, and histology. Male and female mice were used to comply with 3R policy to reduce animal use and data was pooled for analysis.

Rat model with chronic kidney disease (CKD) induced vascular calcification - This study used a well-characterized rat model with adenine induced CKD. [35, 44] 7-week-old male Wistar rats (225-250 g, Charles River, Lille France) were used to avoid interference with hormonal effects and because they are more vulnerable to the development of CKD. Rats were housed 2 per cage and randomly assigned to different groups. An equilibration period of 3 weeks was used to ensure a body weight of approximately 320g at the start of the study. CKD was induced by maintaining the rats on an adenine diet containing 0.75 % adenine (Acros Organics) with a 0.92 % phosphorous and 1 % calcium content in combination with a low protein content (2.5 %). A control group (n=6) with normal renal function was included and maintained on a control diet. The CKD groups were sacrificed weekly starting from week 1 and then 2, 3, 4 and 8 after the diet was introduced. The control group rats with normal diet were sacrificed at the end of the experiment (week 8).

Adenoviral constructs and transfections - Adenovirus (Cyagen Biosciences) expressing recombinant FLAG-tag Runx2 (FL-Runx2), a short hairpin RNA against Runx2 mRNA (shRunx2) or enhanced green fluorescent protein (EGFP) were used to transduce VSMCs at 70 % confluence. Multiplicity of infection was 10 particles per cell, routinely achieving >80 % transduction efficiency as assessed by control EGFP. For Small interfering RNA–mediated interference of Ku70, sc29383 (Santa Cruz biotech) was transfected into VSMCs using HiPerfect transfection reagent (Qiagen).

Antibodies - Primary antibodies used were as follows: Runx2 (D130-3) (MBL International); Runx2 (sc-10758), p53 (sc-126) (Santa Cruz Biotech); FLAG (M2, F3165), H2AX (PLA0294), ß-actin (AC-74) (Sigma Aldrich); 8-OxodG (N45.1) (JaICA); FLAG (ab1257), Ku70 (ab83501), ERK 1/2 (ab36991), pERK (ab201015), pY142 H2AX (ab94602), α Smooth muscle actin (ab7817), Runx2 (ab23981) (abcam); γH2AX (2577), Lamins A/C (2032), Chk2 (2662), pChk2 (T68) (2197), Cleaved caspase-3 (Asp175) (9661) (Cell Signaling Technology, Danvers, Mass); PAR (4336-APC-050) (Novus Biologicals).

TUNEL staining - TUNEL staining assays were carried out using a commercially available kit according to the manufacturer's instructions (abcam; ab206386).

Calcification assays - For Alizarin red S staining, VSMCs were washed with PBS and fixed in 4 % formaldehyde in PBS for 10 mins at 21 °C. VSMCs were then washed with dH_2O and then incubated with 2 % Alizarin red S (Sigma-Aldrich) for 5 mins then briefly rinsed with water prior to imaging. o-Cresolphthalein assays on VSMCs were performed as previously described. [42] Adenovirus was used to knock-down Runx2 (shRunx2), over-express Runx2 (FL-Runx2) or express EGFP (control). To harvest cells from mouse models, 3 mm of thoracic aorta for each mouse was collected and washed in HBSS. To extract Ca^{2+}, the aortas were placed in a Dounce Glass Tissue Homogenizer with 200 µl 0.1 M HCl and homogenised every 30 mins for 2 hours. The homogenate was centrifuged at 13000 x g for 2 mins and subject to o-Cresolphthalein assay for calcium analysis.
Immunoblotting - Total cell extracts were prepared by washing VSMCs in ice cold PBS then scraping into fresh ice cold PBS and centrifugation at 700 x g for 5 mins. Pellets were resuspended in lysate buffer (10 mM Tris pH 7.5, 150 mM NaCl, 1 mM EDTA, 1% Triton X-100, protease inhibitors) and sonicated for 10 seconds followed by centrifugation at 700 x g for 5 min. 0.01 % bromophenol blue, 200 mM DTT , 4 % SDS and 20 % glycerol were added to lysates prior to boiling for 5 mins and separation by SDS-PAGE, transfer to PVDF membrane, blocking and primary antibody incubation. Secondary antibodies conjugated to IRDye 800CW (LI-COR Biosciences) were then used followed by detection and quantification with an imager (Odyssey; LI-COR Biosciences).

Immunofluorescence - VSMCs were cultured on coverslips and fixed in 4 % paraformaldehyde in PBS for 10 mins at 21 °C followed by 3 min permeabilisation with 0.5 % NP-40 in PBS. Coverslips were then blocked (3 % BSA in PBS) for 1 hour at 21 °C before incubation with primary antibodies in blocking solution for 12 hours at 4 °C in a humidifying chamber. Coverslips were washed in PBS followed by 1 hour 21 °C incubation with fluorescent dye conjugated secondary antibodies (Invitrogen). Coverslips were washed with PBS, mounted onto slides with medium containing DAPI, and z-stacks were obtained using a Nikon A1R confocal microscope with NIS-Elements software. Different channels were acquired sequentially. For mice thoracic aortas, 10 µm thick cryosections were stained and imaged using an Olympus IX-81 microscope.

Comet assays - VSMCs were cultured to approximately 70 % confluency then were washed with ice-cold PBS, trypsinised and resuspended in 0.6 % low melting point agarose then dispensed in duplicate onto pre-coated slides and allowed to set on ice for 20 mins in the dark. Slides were then transferred into ice-cold lysis buffer (100 mM EDTA, 2.5 M NaCl, 10 mM Tris pH10, 1% Triton X-100) for 1 hour, washed twice with ice-cold dH_2O followed by electrophoresis in ice cold buffer (300 mM NaOH, 1 mM EDTA) at 20 V for 30 mins. Slides were then submerged in neutralisation buffer (0.4 M Tris pH 7.5), washed with dH_2O and dried prior to staining with Nancy-520 (Sigma Aldrich) and imaging by confocal microscopy.

Immunohistochemistry - Immunohistochemistry was performed on Wistar rat thoracic aortas. 4 µm or 7 µm thick sections were paraffinized, rehydrated, restored for immunoreactivity, blocked for endogenous peroxidase activity and nonspecific binding and then were incubated with primary antibodies. The biotinylated secondary antibodies, avidin-biotin complex amplification (PK-6101 & PK-6102; Vector laboratories) and DAB peroxidase substrate kit (SK-4100; vector laboratories) were used to develop the staining. Sections were then counterstained with hematoxylin and mounted using DPX following dehydration. Images were taken using a Leica ICC50 W microscope. Mineral deposition and expression of γH2AX, 8-oxodG and Runx2 were quantified using ImageJ software. Calcification was

quantified using a threshold measure method and expression of γH2Ax, 8-oxodG and Runx2 by enumerating positive (brown) and negative (purple) cells.

RNA isolation and quantitative reverse transcription polymerase chain reaction (RT-qPCR) – RNA from human VSMCs was isolated from cells using STAT60 (CS-110, AMS Biotechnology), followed by cDNA synthesis using Mu-MLV reverse transcriptase (ME-0125-10, Eurogentec). qPCR was performed in triplicate using qPCRBIO SyGreen Mix (PCR Biosystems). Reactions were carried out in a StepOnePlus Real Time PCR System (Applied Biosystems). Primers used are as follows: *Runx2* (Runx2) (QT00020517), *CDKN1A* (p21) (QT00062090), *GAPDH* (GAPDH) (QT00079247), *Sp7* (Osterix) (QT00213514), *MMP9* (MMP9) (QT00040040) (Qiagen). Other primers used were: *BGLAP* (Osteocalcin) (5'-GGCAGCGAGGTAGTGAAGAG-3' and 5'-CGATAGGCCTCCTGAAAGC-'3) and *IBSP* (BSP) (5'-AGTTTCGCAGACCTGACATCCAGT-3' and 5'-TTCATAACTGTCCTTCCCACGGCT-3'). Expression levels of target genes were all corrected using GAPDH expression. PCRs were performed in 20 µl reaction volumes at 95 ºC for 10 min followed by 40 cycles at 95 ºC for 5 seconds and 60ºC for 1 min. RNA was extracted from mouse aorta by homogenising vessels in 1 ml TRIzol (Invitrogen) using matrix D beads (MP Biomedicals) in a Precellys 24 tissue homogeniser (Bertin Technologies). cDNA synthesis and qPCR were performed as described above but using the following primers: *Runx2* (QT00102193), *GAPDH* (QT01658692), *IBSP* (QT00115304), *Sp7* (QT00293181) and BGLAP (QT01744330) (Qiagen).

Proximity ligation assay - Duolink® In Situ Red Starter Kit Mouse/Rabbit (Sigma Aldrich) was used according to the manufacturer's instructions. Staining was visualised using a Nikon A1R confocal microscope.

Active Caspase 3 ELISA - Active Caspase 3 (Asp175) Human ELISA (ab168541) (abcam) was performed according to the manufacturer's instructions.

Chromatin immunoprecipitation (ChIP) - ab500 ChIP Kit (abcam) was used according to the manufacturer's instructions. Briefly, VSMCs were trypsinised, centrifuged and then washed in ice-cold PBS. Cells were centrifuged again and then fixed in 1.1 % formaldehyde in PBS. Reactions were quenched with glycine and cells were washed in ice cold PBS before being lysed. Chromatin was sheared to approximately 500-1500 bp fragments using a sonicator at 4 °C. Chromatin was diluted and input chromatin was collected. Remaining chromatin was used for ChIP using 4 µg Runx2 (D130-3) as antibody of interest, 4 µg anti-histone H3 as a positive control and no antibody as a negative control. Antibodies were added for 12 hours at 4 °C and then Protein A sepharose beads were used to precipitate protein/DNA complexes. Cross-links were reversed by heating at 98 °C followed by proteinase K addition and DNA purification. Samples were analysed by pPCR. Primers used are as follows: Runx2 (5'-TGTGATACAGTCCAAAGATGTGA-3' and 5'-CCTGTAAGGTTAAGCATTTGTAGAG-3'), p21 (5'-TGCTAGGAACATGAGCAAACT-3' and 5'-TCAGCAGTGGCACAATCTC-3'), BSP (5'-GGGCCACATAAATGGACAATA-3' and 5'-TCATTTGATGTTTCCTCCTGAA-3'), Osterix (5'-CCTTGCCTATCTGCTTCTCTTT-3' and 5'-GTCCTGGATCCAAGCTTCAAA-3'), MMP9 (5'-CCAATCACCACCATCCGTT-3' and 5'-ACAGCAGACATGGCTTTACTC-3'), OCN (5'-AAATACAGAATTAGCCAGGCAT-3' and 5'-AAGAAGCAAGAGAAACAAAGTG-3').

Biochemical fractionation - VSMCs were incubated in fractionation buffer (10 mM HEPES pH 7.9, 10 mM KCl, 1.5 mM $MgCl_2$, 0.5 mM DTT, 0.05% NP40, protease inhibitors and

phosphatase inhibitors on ice for 30 mins with occasional agitation. Following centrifugation at 1,500 x g for 5 mins at 4 °C, the supernatant was collected (cytoplasmic) and the pellet was extracted with ice cold high-salt buffer (20mM Tris-HCl, (pH 8.0), 420 mM NaCl, 0.5 % NP40, 0.1mM EDTA, 10% glycerol) for 45 mins on ice. Samples were centrifuged at 13,500 x g for 15 mins and the supernatant that contained chromatin-bound proteins was collected (chromatin fraction). The resultant pellet was resuspended in lysate buffer (above), sonicated for 10 seconds and centrifuged at 1,500 x g for 5 mins at 4 °C. The supernatant was collected (nuclear insoluble fraction).

Co-Immunoprecipitation (Co-IP) assays - VSMCs were washed in PBS, harvested and lysed in 10 % glycerol, 0.5 mM EDTA, 25 mM Tris-HCL (pH 7.5), 1 mM Na_2VO_3, 180 mM NaCl, 10 mM β-glycerophosphate, 0.1 mM DTT and 0.1 % NP-40. Lysates were incubated with 4 µg anti-H2AX, rotating at 4 °C, for 12 hours. Protein G agarose beads (Sigma) were then added to the lysates, washed 3x in lysis buffer and boiled for 10 minutes prior to analysis by gel electrophoresis and western blot.

Boronate bead pull-down assays (BBPDAs) of PARylated proteins – Beads coated in boronic acid resins bind to various oligonucleotides via vicinal diols. The chemical nature of poly(ADP-ribose) means PARylated proteins are a strong substrate for these beads and can be pulled-down effectively in BBPDAs. [45] 6 hours prior to *BBPDAs*, cells were treated with Poly(ADP-ribose) glycohydrolase (PARG) inhibitor PDD00017273 (Sigma) to prevent PAR degradation, and any DNA damage treatments were performed. Nuclear fractions were collected as described in "Biochemical fractionation protocol" and this fraction was sonicated in lysate buffer (above) containing PARG inhibitor and mixed with m-aminophenylboronic acid agarose (# A8312, Sigma) for 1 hour at room temperature. Following this incubation, beads were washed twice in SDS wash buffer (1 % SDS, 100 mM HEPES (pH 8.5), 150 mM NaCl) and twice in non-SDS wash buffer (100 mM HEPES (pH 8.5), 150 mM NaCl). Proteins were eluted from beads by boiling for 10 mins and analysed by western blot. For *BBPDAs* using protein from mouse aorta, vessels were homogenised in lysate buffer containing PARG inhibitor followed by sonication (3 x 10 seconds) and centrifugation at 2600 x g and 4 °C for 5 mins. 950 µg of protein was used in each reaction for as described above.

Statistical analysis - Results are presented as mean ± SEM Statistical analysis was performed with GraphPad software. All data was tested for normalcy using the Shapiro-Wilk test prior to comparison analysis. For comparisons of multiple groups; one-way ANOVA with Tukey's test was used. For comparison of just two independent samples the parametric *Student* t-test was used. On graphs, * = $P < 0.05$, ** = $P < 0.01$ *** = $P < 0.001$, **** = $P < 0.0001$. Results were taken from a minimum of 3 independent experiments (technical replicates) using 3 different VSMC isolates (biological replicates). For histology, all groups were compared with the control group. The comparison was made using one-way ANOVA test except for γH2AX where Kruskal Wallis test was used.

Results

DNA damage augments VSMC calcification in a Runx2-dependent manner

Primary human VSMCs cultured in calcifying media containing elevated Ca^{2+} and P_i exhibited visible signs of calcification after 5 days and were highly calcified after 15 days (Figure 1A and S.IA). Western blot (WB) and immunofluorescence (IF) showed increased levels of the DNA damage marker γH2AX (Figure 1B and C and S.IB-G) in calcified VSMCs after 10 days of calcification treatment, and comet assays confirmed the presence of increased physical DNA damage in these cells (Figure 1D and S.IH). Increased Runx2 protein levels (Figure 1B and S.II) and concomitant loss of the smooth muscle marker SMA mirrored the induction of DNA damage and calcification.

To examine whether genomic stress could promote VSMC calcification, and if this was dependent on Runx2, o-Cresolphthalein assays were performed on VSMCs cultured in control or calcifying media in the presence or absence of the DNA damaging agents H_2O_2 (causes oxidative DNA damage) or etoposide (causes DNA double-strand breaks (DSBs)). In addition, levels of Runx2 were manipulated using adenoviral vectors (S.IJ and K). We found DNA damage alone did not induce VSMC calcification but both agents augmented calcification when VSMCs were cultured in calcifying media (Figure 1E and F and S.IL -O). Knock-down of endogenous Runx2 via shRNA interference (shRunx2) had a minimal effect on reducing calcification induced by calcification media alone, however the enhanced calcification caused by H_2O_2 or etoposide was completely abolished (Figure 1E and F). Conversely, adenovirus mediated over-expression of a FLAG-tagged recombinant form of Runx2 (FL-Runx2) increased calcification in calcifying media alone and this increase was further enhanced with additional DNA damage caused by H_2O_2 or etoposide (S.IL and M). These data suggest that Runx2 is not essential for the initiation of VSMC calcification by elevated Ca^{2+} and P_i over this time-course, but Runx2 is pivotal in exacerbating calcification when genomic instability is high.

Increased calcification in response to genomic stress corresponded with enhanced transcription of Runx2 osteogenic targets. RT-qPCR showed expression of *IBSP* (BSP), *Sp7* (Osterix) and *BGLAP* (OCN) were greatest in VSMCs grown in calcifying media supplemented with H_2O_2 with a small but significant increase in expression also seen in response to H_2O_2 treatment alone (Figure 1G-I). Runx2 depletion modestly suppressed expression of these genes in VSMCs cultured in calcifying media alone but more profoundly blocked the baseline and synergistic effects of H_2O_2. We also observed Runx2 dependent increased expression of *IBSP*, *Sp7* and *BGLAP* in response to etoposide treatment (S.IP-R), showing Runx2 activity is also stimulated by DNA DSBs. Additional putative Runx2 target genes *CDKN1A* (p21) and *MMP9* (MMP9 protein) were also tested (S.IS and T) and although these genes increased expression in response to DNA damage and calcifying conditions respectively, these changes were not dependent on Runx2. These data suggest that Runx2 osteogenic activity is most profound when genomic stress is applied to cells and that specific osteogenic targets may be preferentially expressed in response to genotoxic stress.

DNA damage dependent Runx2 accumulation, osteogenic gene expression and VSMC calcification are reduced by PARP and ATM inhibitors

To determine how Runx2 was influenced by genotoxic stress, VSMCs were exposed to either H_2O_2 or etoposide and levels of Runx2 protein were quantified using WB (Figure 2A-C and S.IIA-C) and IF (S.IIC). These experiments revealed a significant increase in Runx2 protein levels following 3 hours of treatment that corresponded to increases in γH2AX. This was despite there being no change in Runx2 gene expression on qRT-PCR (S.

IID), suggesting a post-transcriptional mechanism was likely increasing Runx2 protein levels in response to DNA damage.

To identify potential signalling pathways that could post-translationally elevate Runx2 protein following genotoxic stress, VSMCs were exposed to the same stressors but with the inclusion of inhibitors of DDR proteins PARP1/2 (PJ34) and ATM (Ku55933). These inhibitors were tested alongside inhibitors of ERK signalling (UO126); as this pathway has previously been implicated in VSMC calcification and Runx2 phosphorylation. [46, 47] We observed that PARP and ATM inhibitors effectively blocked the increase in Runx2 protein in response to DNA damage, however ERK inhibition did not (Figure 2D-F and S.IIE-G).

Consistent with the inhibitory effects of PJ34 and Ku55933 on Runx2 protein levels, these inhibitors also reduced VSMC calcification in response to calcifying media and completely blocked the augmented calcification induced by genotoxic stress (Figure 2G). Again, ERK inhibition had no effect. Reduced calcification also corresponded with reduced expression of Runx2 osteogenic target genes as evidenced by marked reductions in *IBSP*, *Sp7* and *BGLAP* expression in VSMCs cultured in calcifying media, with the largest decrease seen in VSMCs cultured in calcifying media supplemented with H_2O_2.

The DDR causes enhanced Runx2 binding to osteogenic target gene promoters and changes its nuclear compartmentalisation.

We next assessed Runx2 occupancy at promoter regions of selected targets in VSMCs in response to genotoxic stress using ChIP assays and observed that Runx2 binding to osteogenic gene promoters *IBSP*, *Sp7* and *BGLAP* was significantly increased by exposure to either H_2O_2 or etoposide (Figure 3A and B and S.IIIA). However, Runx2 binding to its own promoter, *CDKN1A* or *MMP9* promoter regions did not change with either treatment, consistent with the unresponsiveness of these genes to Runx2 depletion (S.IS and T). Both DDR inhibitors PJ34 and Ku55933 were effective at attenuating this increased binding (Figure 3C-E). The DNA repair factor Ku70 has been reported to regulate Runx2 mediated transactivation of some osteogenic targets [48] but we saw no change upon Ku70 depletion (S.IIIB and C), suggesting it was not regulating increased Runx2 binding to osteogenic targets in response to genotoxic stress.

To further investigate how genomic stress influenced Runx2 compartmentalisation, we used cell fractionation on VSMCs treated with H_2O_2 and observed that in response to oxidative stress there was an increase in Runx2 specifically in the chromatin fraction (Figure 3F and S.IIID). Treatment with PJ34 blocked this shift and resulted in retention of more Runx2 in the nuclear soluble fraction, showing that DNA damage affects Runx2 positioning within the nucleus and this is dependent on PARP signalling.

Runx2 localises to sites of DNA damage induced by both etoposide and H_2O_2

The dynamic changes in compartmentalisation in response to DNA damage led us to examine whether Runx2 may also play a functional role within the DDR. Using IF, we observed that both recombinant FL-Runx2 and endogenous Runx2 accumulated at sites of oxidative DNA damage caused by H_2O_2 and at DNA DSBs induced by etoposide (Figure 4A-C and S.IVA-H), with approximately 40% of γH2AX associated with endogenous Runx2 foci.

Proper regulation and amplification of γH2AX is necessary for the integrity of the DDR and recruitment of repair factors. An important requirement for this is the dephosphorylation of an adjacent tyrosine 142 (pY142-H2AX) that in unstressed cells is constitutively phosphorylated. [49-51] Extensive DNA damage can result in retention of pY142-H2AX which suppresses DNA repair pathways and results in apoptosis. [50, 52] IF of Runx2 and pY142-H2AX revealed a degree of colocalisation (S.IVG). Further analysis using triple

staining to visualise the spatial organisation of Runx2 and pY142-H2AX together with γH2AX (Figure 4C and S.IVH) showed that the Runx2/γH2AX complexes were arranged such that aggregations of Runx2 spatially separated H2AX histones presenting either the S139 or Y142 phosphorylated residues. Proximity ligation assays were used to further probe these arrangements and revealed that endogenous Runx2 interacted with both γH2AX and pY142-H2AX (Figure 4D and S.IVI and J) and that following genotoxic stress, significantly more Runx2/γH2AX interactions were detected (VSMCs with more than 15 observable interactions increased from approximately 0 % to 70 %) in conjunction with fewer Runx2/pY142-H2AX interactions (VSMCs with more than 15 observable interactions decreased from approximately 65 % to 15 %).

DNA damage induced Runx2 accumulation promotes pY142-H2AX and apoptosis

The close association between Runx2 and both γH2AX and pY142-H2AX led us to probe whether Runx2 influences either phosphorylated species. WB was used to test how depletion or over-expression of Runx2 affected γH2AX levels in VSMCs after H_2O_2 treatment (Figure 5A and S.VA-D). Compared to controls expressing EGFP, VSMCs treated with shRunx2 exhibited higher γH2AX at baseline and after H_2O_2 treatment. Conversely, over-expression of Runx2 (FL-Runx2) appeared to repress γH2AX, intimating that either these cells had less DNA damage or that γH2AX signalling had been attenuated and uncoupled from actual levels of DNA damage. To delineate this, comet assays were performed (Figure 5B and S.VE) which demonstrated high levels of DNA damage in all samples treated with H_2O_2, supporting that elevated Runx2 protein acted to repress γH2AX. Moreover, both depletion and over-expression of Runx2 caused more DNA damage at baseline, inferring the DDR had become deregulated in both instances.

Next we explored how Runx2 might affect the relationship between γH2AX and pY142-H2AX as a potential mechanism that would account for uncoupling of the DDR and actual DNA damage. Using WB we quantified how both modifications changed in human VSMCs in response to H_2O_2 treatment and observed that upon application of stress, a reduction in pY142-H2AX occurred concurrently with γH2AX accrual (S. VF-H). We then investigated how Runx2 influenced this switch and observed that VSMCs expressing FL-Runx2 retained more pY142-H2AX after H_2O_2 (Figure 5C-E and S.VI). Conversely, depletion of Runx2 resulted in less pY142-H2AX in both stressed and unstressed conditions. Analysis of γH2AX and pY142-H2AX levels in primary VSMCs derived from smooth muscle specific Runx2 knockout mice revealed similar findings, with unstressed cells presenting with higher γH2AX and lower pY142-H2AX compared to controls and markedly higher γH2AX following H_2O_2 (S.VJ-M).

The above data supported a mechanism whereby high levels of Runx2 favoured pY142-H2AX and repressed γH2AX even when DNA damage was present. As this configuration is associated with apoptosis via c-Jun N-terminal protein kinase (JNK) signaling, [50] we used an active caspase-3 assay to assess levels of apoptosis and found over-expression of Runx2 led to increased levels of cleaved caspase-3 (CC3) (Figure 5F and S.VN). These levels were amplified further when H_2O_2 was present. Co-immunoprecipitation assays showed that over-expression of Runx2 increased the amount of JNK proteins interacting with H2AX (Figure 5G and S.VO) under genomic stress, which would be anticipated if Runx2 promotes apoptosis via repression of the DDR and subsequent recruitment of JNK.[52]

Runx2 is PARylated in response to genotoxic stress and PARP inhibitors block its localisation at sites of DNA damage

The marked effect of DDR inhibitors upon Runx2 activity led us to test if localisation of Runx2 at sites of DNA damage was affected when DDR signalling was impaired. As ATM inhibitors would directly suppress γH2AX phosphorylation we focused on the effect of PARP inhibition. In order to mitigate the anticipated lower levels of Runx2 following PARP inhibition under genotoxic stress, we investigated interactions between γH2AX and over-expressed FL-Runx2. We identified significantly fewer cells that contained 15 or more interactions between γH2AX and FL-Runx2 after etoposide treatment in cells treated with PJ34 (Figure 6A), implying PARP activity is involved in Runx2 localisation to sites of DNA damage.

Recent evidence has emerged that PARylation of Runx3 is necessary for its involvement in repair of cross-links in DNA. [53] The two sites within the Runx3 protein that were previously identified as being subject to PARylation [54] are conserved within Runx2 (Figure 6B) leading us to test whether PARylation of Runx2 was responsible for its increased stability in response to DNA damage. For this, boronate bead pull-down assays (*BBPDAs)* using beads that attach to covalently bound PARylated residues [45] were performed. These experiments showed that significantly more endogenous Runx2 was pulled-down from VSMCs cultured in calcifying media, H_2O_2 or etoposide compared to controls (Figure 6C and S.VIA) and that PJ34 abolished this increase in all instances. As late passage presenescent VSMCs exhibit more DNA damage and endogenous Runx2 accumulation, as well as osteogenic differentiation, [33] we also tested if there was more PARylated Runx2 in these cells and *BBPDAs* confirmed this was the case (S.VIB and C).

To further confirm that genomic stress directly induced PARylation of Runx2 we repeated *BBPDAs* in VSMCs expressing FL-Runx2. This allayed the possibility that the higher incidence of endogenous PARylated Runx2 pull-down that was observed was caused by differences in total Runx2 protein levels resulting from different treatments. As the total input of FL-Runx2 was the same in stressed or non-stressed cells, any increase in Runx2 pulled-down would be evidence of Runx2 PARylation. As shown in Figure 6D-E and S.VID-E, induction of DNA damage by H_2O_2 or etoposide resulted in increased PARylated Runx2 and this was abolished in the presence of the PARP inhibitor PJ34. Inhibition of ATM also lowered levels of PARylated FL-Runx2 after genotoxic stress (Figure 6F and S.VIF), suggesting ATM activity is upstream of this modification.

Runx2 localizes with γH2AX in calcified arteries and is essential for osteogenic gene expression in vivo

To analyse the relationship between Runx2 and DNA damage during calcification *in vivo,* immunohistochemistry was performed on the aorta of rats using a model where calcification is induced by dysregulated mineral metabolism caused by chronic renal failure. Calcification occurred at week 4 after induction and at this timepoint levels of DNA damage, shown by increased γH2AX and 8-oxodG staining, peaked, as did the accumulation of nuclear Runx2 (S.VIIA). Moreover, VSMCs positive for these markers were in close proximity to calcified regions. At week 8 there was a reduction in cells positive for Runx2 and DNA damage markers, which may be explained by apoptosis of Runx2 positive VSMCs at sites of calcification.

To examine this further in a more dynamic model of vascular calcification, wild-type (*Runx2*$^{f/f}$) and smooth muscle-specific *Runx2* Knock-Out mice (*Runx2*$^{\Delta SM}$) were treated with vitamin D (VitD) to induce mineral dysregulation and aortic calcification. As anticipated, VitD treatment increased levels of Runx2 in the aorta of *Runx2*$^{f/f}$ mice but this was greatly attenuated in *Runx2*$^{\Delta SM}$ mice (Figure 7A and S.VIIB). Using immunohistochemistry, we

found that VitD treatment induced elevated levels of DNA damage as shown by increased γH2AX staining in the aorta of both *Runx2*$^{f/f}$ and *Runx2*$^{\Delta SM}$ (Figure 7B and S.VIID), however we were unable to detect significant alterations in pY142-H2AX as levels were highly variable (data not shown).

Runx2$^{\Delta SM}$ mice were resistant to calcification as shown by the absence of von Kossa positive staining in the aorta after VitD treatment (Figure 7B) and also reduced calcium accumulation in o-Cresolphthalein assays (S.VIIC). Consistent with Runx2 driving apoptosis in response to higher levels of DNA damage, quantification of CC3 (which gives a snapshot of apoptosis) showed that VitD caused a significant increase in apoptotic cells in *Runx2*$^{f/f}$ animals but not in *Runx2*$^{\Delta SM}$ mice (S.7E). Conversely TUNEL staining revealed high staining in *Runx2*$^{\Delta SM}$ mice after VitD treatment (S.VIIF) most likely indicative of DNA breaks which is consistent with sustained and elevated DNA damage due to destabilisation of the DDR [55] in *Runx2*$^{\Delta SM}$ mice.

RT-qPCR for Runx2 and its targets in mice with or without VitD treatment showed Runx2 expression was low in *Runx2*$^{\Delta SM}$ mice and modestly increased in *Runx2*$^{f/f}$ mice in response to VitD. Increased expression of Runx2 targets including *Runx2* itself, *IBSP*, *Sp7* and *BGLAP* was induced in control animals in response to VitD but not in *Runx2*$^{\Delta SM}$ mice (Figure 7C-F). However, as seen during *in vitro* studies, other Runx2 targets *CDKN1A* and *MMP9* showed no difference in expression between *Runx2*$^{f/f}$ or *Runx2*$^{\Delta SM}$ mice (S.VIIG). To ascertain if increased osteogenic differentiation was associated with increased PARylation of Runx2 *BBPDAs* were again employed (Figure 7G). These showed higher levels of PARylated Runx2 in VitD treated *Runx2*$^{f/f}$ mice that was not observed in *Runx2*$^{\Delta SM}$ mice, supporting the notion that genomic stress induced PARylation of Runx2 leads to activation of a subset of specific osteogenic targets to enhance calcification.

Discussion

Runx2 in the DDR and biomineralization

This study has delineated for the first time how Runx2 governs VSMC phenotype in response to genomic stress and identifies ATM and PARP signalling as key drivers of calcification. Runx2 was identified as a component of the DDR where it localised to sites of DNA damage where its role in regulating H2AX phosphorylation events was tightly coupled to VSMC osteogenic reprogramming and JNK mediated apoptosis. Previous studies have robustly demonstrated that a combination of VSMC phenotypic switching and apoptosis work in concert to drive calcification [14, 56] but this study is the first to implicate Runx2 in driving both these processes with these activities dependent on activation of the DDR.

Runx2 regulates the DDR and couples it to transcriptional reprogramming

In vitro, agents that caused genotoxic stress accelerated VSMC calcification and this correlated with Runx2 accumulation and increased osteogenic activity both of which were blocked by DDR inhibitors. Similarly *in vivo,* calcification induced by dysregulated mineral metabolism due to CKD or vitamin D overload was associated with DNA damage and Runx2 accumulation at calcified sites. This was temporally associated with activation of osteogenic genes and apoptosis. In the absence of Runx2, osteogenic differentiation, apoptosis and calcification were ameliorated.

The accumulation of Runx2 in response to genotoxic stress correlated with its PARylation both *in vitro* and *in vivo* in calcified arteries. *In vitro* studies showed that this modification was required for its localisation to sites of DNA damage, increased promoter occupancy and activation of specific osteogenic targets. Inhibition of the DDR using either

ATM or PARP inhibition blocked Runx2 localization to sites of DNA damage, osteogenic responses and calcification.

Genomic stress led to increased chromatin association of Runx2 and specific activation of osteogenic targets, however the mechanisms linking Runx2 function in the DDR with osteogenic cell fate are unknown. We ruled out a role for the DDR-dependent transcriptional co-factor Ku70 [48] although it is possible that other Runx2 binding partners may regulate target specificity. [57] Another plausible explanation could be linked to its association with the nuclear matrix. This scaffold can regulate chromatin organisation and histone modifications [58, 59] which are important for both transcription and the DDR. Previous studies have shown that Runx2 can recruit chromatin-modifying proteins including BAZ1B protein to sites of DNA damage in cancer cells. [24] In addition, Runx2 can regulate expression of a number of epigenetic modifiers including EZH2 [60] that modulate gene expression at multiple sites across the genome. A combination of these functions might allow global epigenetic modifications to drive changes in gene expression in response to DNA damage. Further analysis of Runx2 targets in VSMCs is required to confirm these mechanisms and target specificity.

Runx2, DDR signalling and apoptosis

Until now, understanding of the involvement of Runx2 in the DDR has been limited. [24, 29, 61, 62] Conversely, more precise functions for Runx1 and 3 have been documented. Both are PARylated in response to genome damage [53, 63] and bind to DNA repair structures. Runx3 has a recognised role in DNA cross-link repair and interacts with the RecQ helicase BLM to recruit FANCD2, [53] with this function being blocked by PARP inhibitors. We observed that Runx2 is also PARylated following DNA damage and this was necessary for its localization to DNA repair sites. Here it led to retention of pY142-H2AX and suppression of γH2AX levels even after DNA damage induction. The co-phosphorylation of both γH2AX and pY142-H2AX is associated with DNA repair repression and initiation of apoptosis through recruitment of the pro-apoptotic factor JNK to H2AX. [50] It is thought that duel phosphorylation of both residues prevents binding of key DNA repair scaffold protein MDC1 [64] and inhibition of DNA repair. In this scenario, unrepaired DNA damage will accumulate and this stimulates JNK translocation into the nucleus and subsequent phosphorylation of substrates involved in caspase-activated DNase degradation of DNA, including H2AX. [65] This process is mediated by PTB-domain protein Fe65 which binds to pY142-H2AX under conditions of stress and recruits JNK. [50] How Runx2 promotes pY142-H2AX under genotoxic stress conditions and induces this apoptotic pathway remains to be elucidated, however it would be important to investigate if Runx2 influences the activities of the phosphatase Eya [50] or WSTF kinase, [49] both of which determine Y142-H2AX phosphorylation. Our data suggested that elevated levels of Runx2 were required to drive this apoptotic process suggesting that chronically elevated genotoxic stress - as observed in ageing and disease - might be requisite to induce this activity.

Whilst the precise cue that dictates whether Runx2 favours VSMC osteogenic transition or induction of apoptosis is not certain, we propose that the amount and persistence of DNA damage is likely an important factor, with more and prolonged damage favouring cell death (S. VIII). Interestingly, JNK mediated apoptosis has been documented to be associated with development, [66] so whether pro-apoptotic activity of Runx2 is also present in the bone growth plate - where γH2AX positive cells have been recorded [35] - would be important to investigate as this would suggest that the coupling of DNA damage, osteogenic transcription and apoptosis via Runx2 are also key to bone development.

The DDR as a therapeutic target for calcification

In this study we have underlined a key role for the activation of Runx2 by genomic stress during vascular biomineralization. We observed that arresting DDR signalling via either ATM or PARP inhibition blocked DNA-damage dependent Runx2 PARylation and VSMC calcification, and our data supports a model whereby ATM activity is upstream of the PARPs responsible for PARylation of Runx2. Previous studies have shown synergistic activity of these enzymes, in the case of recruitment of Kif2C to DNA damage [67] and also in the formation of ATM and PARP1 complexes that influence cross-talk between DDR signalling pathways. [68] Although further work is required to determine how these pathways might intersect during VSMC calcification and regulate Runx2 activity, our data does highlight the potential of inhibitors of the DDR as therapeutics for vascular calcification. In addition, we speculate that DDR activation of Runx2 may also be important in a number of other contexts where DNA damage and senescence have been linked to ectopic calcification including atherosclerosis, [35] diabetic vasculopathy, [69] age and radiation-induced aortic stenosis [70] as well as senescence associated mineralization of skeletal muscle [71] and connective tissues. [22, 23] We also speculate that activation of Runx2 by the DDR may be important for normal bone formation but further exploration into these possibilities is now required. Taken together our data indicate that Runx2 exhibits characteristics of an antagonistic pleiotropic gene, with its important role during bone development outweighing a detrimental function as a promoter of ectopic mineralization.

Acknowledgements

Work by AC, SA, SY, RH, MS was supported by a British Heart Foundation Programme Grant to CS (RG/17/2/32808). AV and PCD were funded by the University of Antwerp.

Author contributions

Conceptualization, A.M.C. and C.M.S.; Methodology, A.M.C., R.H., A.V., P.C.D. and C.M.S.; Formal Analysis, A.M.C., R.H. and S.A.; Investigation, A.M.C., R.H. and S.A.; Resources, R.H., M.S., A.V., P.C.D., and C.M.S.; Writing – Original Draft, A.M.C. and C.M.S.; Writing – Review & Editing, A.M.C., S.Y., R.H, S.A., M.S., A.V., P.C.D. and C.M.S.; Supervision, C.M.S.; Project Administration, C.M.S.; Funding Acquisition, C.M.S. and P.C.D.

Conflicts of interest

The authors declare there are no conflicts of interest to declare.

References:

1. Nicoll R, Henein MY. The predictive value of arterial and valvular calcification for mortality and cardiovascular events. *Int J Cardiol Heart Vessel*. 2014;3:1-5
2. Wayhs R, Zelinger A, Raggi P. High coronary artery calcium scores pose an extremely elevated risk for hard events. *J Am Coll Cardiol*. 2002;39:225-230
3. Aladin AI, Al Rifai M, Rasool SH, Dardari Z, Yeboah J, Nasir K, Budoff MJ, Psaty BM, Blumenthal RS, Blaha MJ, McEvoy JW. Relation of coronary artery calcium and extra-coronary aortic calcium to incident hypertension (from the multi-ethnic study of atherosclerosis). *Am J Cardiol*. 2018;121:210-216
4. Kapustin AN, Chatrou ML, Drozdov I *et al*. Vascular smooth muscle cell calcification is mediated by regulated exosome secretion. *Circ Res*. 2015;116:1312-1323

5. Durham AL, Speer MY, Scatena M, Giachelli CM, Shanahan CM. Role of smooth muscle cells in vascular calcification: Implications in atherosclerosis and arterial stiffness. *Cardiovasc Res*. 2018;114:590-600
6. Steitz SA, Speer MY, Curinga G, Yang HY, Haynes P, Aebersold R, Schinke T, Karsenty G, Giachelli CM. Smooth muscle cell phenotypic transition associated with calcification: Upregulation of cbfa1 and downregulation of smooth muscle lineage markers. *Circ Res*. 2001;89:1147-1154
7. Ozaki T, Yu M, Yin D, Sun D, Zhu Y, Bu Y, Sang M. Impact of runx2 on drug-resistant human pancreatic cancer cells with p53 mutations. *BMC Cancer*. 2018;18:018-4217
8. Javed A, Gutierrez S, Montecino M, van Wijnen AJ, Stein JL, Stein GS, Lian JB. Multiple cbfa/aml sites in the rat osteocalcin promoter are required for basal and vitamin d-responsive transcription and contribute to chromatin organization. *Mol Cell Biol*. 1999;19:7491-7500
9. Ducy P, Zhang R, Geoffroy V, Ridall AL, Karsenty G. Osf2/cbfa1: A transcriptional activator of osteoblast differentiation. *Cell*. 1997;89:747-754
10. Shanahan CM, Cary NR, Salisbury JR, Proudfoot D, Weissberg PL, Edmonds ME. Medial localization of mineralization-regulating proteins in association with monckeberg's sclerosis: Evidence for smooth muscle cell-mediated vascular calcification. *Circulation*. 1999;100:2168-2176
11. Tyson KL, Reynolds JL, McNair R, Zhang Q, Weissberg PL, Shanahan CM. Osteo/chondrocytic transcription factors and their target genes exhibit distinct patterns of expression in human arterial calcification. *Arterioscler Thromb Vasc Biol*. 2003;23:489-494
12. Kapustin AN, Schoppet M, Schurgers LJ, Reynolds JL, McNair R, Heiss A, Jahnen-Dechent W, Hackeng TM, Schlieper G, Harrison P, Shanahan CM. Prothrombin loading of vascular smooth muscle cell-derived exosomes regulates coagulation and calcification. *Arterioscler Thromb Vasc Biol*. 2017;37:e22-e32
13. Lutgens E, de Muinck ED, Kitslaar PJ, Tordoir JH, Wellens HJ, Daemen MJ. Biphasic pattern of cell turnover characterizes the progression from fatty streaks to ruptured human atherosclerotic plaques. *Cardiovasc Res*. 1999;41:473-479
14. Proudfoot D, Skepper JN, Hegyi L, Bennett MR, Shanahan CM, Weissberg PL. Apoptosis regulates human vascular calcification in vitro: Evidence for initiation of vascular calcification by apoptotic bodies. *Circulation research*. 2000;87:1055-1062
15. Jeong JH, Jin JS, Kim HN, Kang SM, Liu JC, Lengner CJ, Otto F, Mundlos S, Stein JL, van Wijnen AJ, Lian JB, Stein GS, Choi JY. Expression of runx2 transcription factor in non-skeletal tissues, sperm and brain. *Journal of cellular physiology*. 2008;217:511-517
16. Takarada T, Hinoi E, Nakazato R, Ochi H, Xu C, Tsuchikane A, Takeda S, Karsenty G, Abe T, Kiyonari H, Yoneda Y. An analysis of skeletal development in osteoblast-specific and chondrocyte-specific runt-related transcription factor-2 (runx2) knockout mice. *Journal of bone and mineral research : the official journal of the American Society for Bone and Mineral Research*. 2013;28:2064-2069
17. Zeng C, McNeil S, Pockwinse S, Nickerson J, Shopland L, Lawrence JB, Penman S, Hiebert S, Lian JB, van Wijnen AJ, Stein JL, Stein GS. Intranuclear targeting of aml/cbfalpha regulatory factors to nuclear matrix-associated transcriptional domains. *Proc Natl Acad Sci U S A*. 1998;95:1585-1589
18. Lin ME, Chen T, Leaf EM, Speer MY, Giachelli CM. Runx2 expression in smooth muscle cells is required for arterial medial calcification in mice. *The American journal of pathology*. 2015;185:1958-1969
19. Lin ME, Chen TM, Wallingford MC, Nguyen NB, Yamada S, Sawangmake C, Zhang J, Speer MY, Giachelli CM. Runx2 deletion in smooth muscle cells inhibits vascular osteochondrogenesis and calcification but not atherosclerotic lesion formation. *Cardiovasc Res*. 2016;112:606-616

20. Sun Y, Byon CH, Yuan K, Chen J, Mao X, Heath JM, Javed A, Zhang K, Anderson PG, Chen Y. Smooth muscle cell-specific runx2 deficiency inhibits vascular calcification. *Circ Res*. 2012;111:543-552
21. Liu L, Zeng P, Yang X, Duan Y, Zhang W, Ma C, Zhang X, Yang S, Li X, Yang J, Liang Y, Han H, Zhu Y, Han J, Chen Y. Inhibition of vascular calcification. *Arterioscler Thromb Vasc Biol*. 2018;38:2382-2395
22. Röhl S, Rykaczewska U, Seime T *et al.* Transcriptomic profiling of experimental arterial injury reveals new mechanisms and temporal dynamics in vascular healing response. *JVS: Vascular Science*. 2020;1
23. Raaz U, Schellinger IN, Chernogubova E *et al.* Transcription factor runx2 promotes aortic fibrosis and stiffness in type 2 diabetes mellitus. *Circulation research*. 2015;117:513-524
24. Yang S, Quaresma AJ, Nickerson JA, Green KM, Shaffer SA, Imbalzano AN, Martin-Buley LA, Lian JB, Stein JL, van Wijnen AJ, Stein GS. Subnuclear domain proteins in cancer cells support the functions of runx2 in the DNA damage response. *J Cell Sci*. 2015;128:728-740
25. Mika S, Rost B. Nmpdb: Database of nuclear matrix proteins. *Nucleic acids research*. 2005;33
26. Okorokov AL, Rubbi CP, Metcalfe S, Milner J. The interaction of p53 with the nuclear matrix is mediated by f-actin and modulated by DNA damage. *Oncogene*. 2002;21:356-367
27. Erdemir T, Bilican B, Oncel D, Goding CR, Yavuzer U. DNA damage-dependent interaction of the nuclear matrix protein c1d with translin-associated factor x (trax). *Journal of cell science*. 2002;115:207-216
28. Qiao F, Moss A, Kupfer GM. Fanconi anemia proteins localize to chromatin and the nuclear matrix in a DNA damage- and cell cycle-regulated manner. *The Journal of biological chemistry*. 2001;276:23391-23396
29. Wysokinski D, Pawlowska E, Blasiak J. Runx2: A master bone growth regulator that may be involved in the DNA damage response. *DNA Cell Biol*. 2015;34:305-315
30. Blyth K, Vaillant F, Hanlon L, Mackay N, Bell M, Jenkins A, Neil JC, Cameron ER. Runx2 and myc collaborate in lymphoma development by suppressing apoptotic and growth arrest pathways in vivo. *Cancer Res*. 2006;66:2195-2201
31. Schnerch D, Lausch E, Becker H, Felthaus J, Pfeifer D, Mundlos S, Engelhardt M, Schwabe M, Wasch R. *Up-regulation of runx2 in acute myeloid leukemia in a patient with an inherent runx2 haploinsufficiency and cleidocranial dysplasia*. Leuk Lymphoma. 2014 Aug;55(8):1930-2. doi: 10.3109/10428194.2013.855310. Epub 2014 Feb 24.
32. Akech J, Wixted JJ, Bedard K, van der Deen M, Hussain S, Guise TA, van Wijnen AJ, Stein JL, Languino LR, Altieri DC, Pratap J, Keller E, Stein GS, Lian JB. Runx2 association with progression of prostate cancer in patients: Mechanisms mediating bone osteolysis and osteoblastic metastatic lesions. *Oncogene*. 2010;29:811-821
33. Liu Y, Drozdov I, Shroff R, Beltran LE, Shanahan CM. Prelamin a accelerates vascular calcification via activation of the DNA damage response and senescence-associated secretory phenotype in vascular smooth muscle cells. *Circulation research*. 2013;112:e99-109
34. Wang X, Li B. Genetic studies of bone diseases: Evidence for involvement of DNA damage response proteins in bone remodeling. *Int J Biomed Sci*. 2007;3:217-228
35. Muller KH, Hayward R, Rajan R *et al.* Poly(adp-ribose) links the DNA damage response and biomineralization. *Cell reports*. 2019;27:3124-3138.e3113
36. Shiloh Y. Atm and related protein kinases: Safeguarding genome integrity. *Nat Rev Cancer*. 2003;3:155-168
37. Rasheed N, Wang X, Niu QT, Yeh J, Li B. Atm-deficient mice: An osteoporosis model with defective osteoblast differentiation and increased osteoclastogenesis. *Hum Mol Genet*. 2006;15:1938-1948
38. Sepe V, Rampino T, Libetta C. Arterial "inflammaging" drives vascular calcification in children on dialysis. *Kidney international*. 2019;96:522

39. Robaszkiewicz A, Erdelyi K, Kovacs K, Kovacs I, Bai P, Rajnavolgyi E, Virag L. Hydrogen peroxide-induced poly(adp-ribosyl)ation regulates osteogenic differentiation-associated cell death. *Free Radic Biol Med*. 2012;53:1552-1564
40. Chow WY, Rajan R, Muller KH, Reid DG, Skepper JN, Wong WC, Brooks RA, Green M, Bihan D, Farndale RW, Slatter DA, Shanahan CM, Duer MJ. Nmr spectroscopy of native and in vitro tissues implicates polyadp ribose in biomineralization. *Science (New York, N.Y.)*. 2014;344:742-746
41. Wang C, Xu W, An J, Liang M, Li Y, Zhang F, Tong Q, Huang K. Poly(adp-ribose) polymerase 1 accelerates vascular calcification by upregulating runx2. *Nature communications*. 2019;10:1203
42. Reynolds JL, Joannides AJ, Skepper JN, McNair R, Schurgers LJ, Proudfoot D, Jahnen-Dechent W, Weissberg PL, Shanahan CM. Human vascular smooth muscle cells undergo vesicle-mediated calcification in response to changes in extracellular calcium and phosphate concentrations: A potential mechanism for accelerated vascular calcification in esrd. *J Am Soc Nephrol*. 2004;15:2857-2867
43. Orita Y, Yamamoto H, Kohno N, Sugihara M, Honda H, Kawamata S, Mito S, Soe NN, Yoshizumi M. Role of osteoprotegerin in arterial calcification: Development of new animal model. *Arteriosclerosis, thrombosis, and vascular biology*. 2007;27:2058-2064
44. Verhulst A, Neven E, D'Haese PC. Characterization of an animal model to study risk factors and new therapies for the cardiorenal syndrome, a major health issue in our aging population. *Cardiorenal medicine*. 2017;7:234-244
45. Zhen Y, Yu Y. Proteomic analysis of the downstream signaling network of parp1. *Biochemistry*. 2018;57:429-440
46. Ding HT, Wang CG, Zhang TL, Wang K. Fibronectin enhances in vitro vascular calcification by promoting osteoblastic differentiation of vascular smooth muscle cells via erk pathway. *Journal of cellular biochemistry*. 2006;99:1343-1352
47. Xiao G, Jiang D, Thomas P, Benson MD, Guan K, Karsenty G, Franceschi RT. Mapk pathways activate and phosphorylate the osteoblast-specific transcription factor, cbfa1. *The Journal of biological chemistry*. 2000;275:4453-4459
48. Willis DM, Loewy AP, Charlton-Kachigian N, Shao JS, Ornitz DM, Towler DA. Regulation of osteocalcin gene expression by a novel ku antigen transcription factor complex. *The Journal of biological chemistry*. 2002;277:37280-37291
49. Xiao A, Li H, Shechter D, Ahn SH, Fabrizio LA, Erdjument-Bromage H, Ishibe-Murakami S, Wang B, Tempst P, Hofmann K, Patel DJ, Elledge SJ, Allis CD. Wstf regulates the h2a.X DNA damage response via a novel tyrosine kinase activity. *Nature*. 2009;457:57-62
50. Cook PJ, Ju BG, Telese F, Wang X, Glass CK, Rosenfeld MG. Tyrosine dephosphorylation of h2ax modulates apoptosis and survival decisions. *Nature*. 2009;458:591-596
51. Krishnan N, Jeong DG, Jung SK, Ryu SE, Xiao A, Allis CD, Kim SJ, Tonks NK. Dephosphorylation of the c-terminal tyrosyl residue of the DNA damage-related histone h2a.X is mediated by the protein phosphatase eyes absent. *The Journal of biological chemistry*. 2009;284:16066-16070
52. Singh RK, Gunjan A. Histone tyrosine phosphorylation comes of age. *Epigenetics*. 2011;6:153-160
53. Tay LS, Krishnan V, Sankar H, Chong YL, Chuang LSH, Tan TZ, Kolinjivadi AM, Kappei D, Ito Y. Runx poly(adp-ribosyl)ation and blm interaction facilitate the fanconi anemia pathway of DNA repair. *Cell reports*. 2018;24:1747-1755
54. Zhang Y, Wang J, Ding M, Yu Y. Site-specific characterization of the asp- and glu-adp-ribosylated proteome. *Nature methods*. 2013;10:981-984
55. Ansari B, Coates PJ, Greenstein BD, Hall PA. In situ end-labelling detects DNA strand breaks in apoptosis and other physiological and pathological states. *The Journal of pathology*. 1993;170:1-8

56. Shroff RC, McNair R, Figg N, Skepper JN, Schurgers L, Gupta A, Hiorns M, Donald AE, Deanfield J, Rees L, Shanahan CM. Dialysis accelerates medial vascular calcification in part by triggering smooth muscle cell apoptosis. *Circulation*. 2008;118:1748-1757
57. Pratap J, Lian JB, Javed A, Barnes GL, van Wijnen AJ, Stein JL, Stein GS. Regulatory roles of runx2 in metastatic tumor and cancer cell interactions with bone. *Cancer metastasis reviews*. 2006;25:589-600
58. Davie JR. The nuclear matrix and the regulation of chromatin organization and function. *Int Rev Cytol*. 1995:191-250
59. Reyes JC, Muchardt C, Yaniv M. Components of the human swi/snf complex are enriched in active chromatin and are associated with the nuclear matrix. *J Cell Biol*. 1997;137:263-274
60. Wu H, Whitfield TW, Gordon JA, Dobson JR, Tai PW, van Wijnen AJ, Stein JL, Stein GS, Lian JB. Genomic occupancy of runx2 with global expression profiling identifies a novel dimension to control of osteoblastogenesis. *Genome biology*. 2014;15:R52
61. Blyth K, Cameron ER, Neil JC. The runx genes: Gain or loss of function in cancer. *Nature reviews. Cancer*. 2005;5:376-387
62. Blyth K, Terry A, Mackay N, Vaillant F, Bell M, Cameron ER, Neil JC, Stewart M. Runx2: A novel oncogenic effector revealed by in vivo complementation and retroviral tagging. *Oncogene*. 2001;20:295-302
63. Jungmichel S, Rosenthal F, Altmeyer M, Lukas J, Hottiger MO, Nielsen ML. Proteome-wide identification of poly(adp-ribosyl)ation targets in different genotoxic stress responses. *Molecular cell*. 2013;52:272-285
64. Stucki M, Clapperton JA, Mohammad D, Yaffe MB, Smerdon SJ, Jackson SP. Mdc1 directly binds phosphorylated histone h2ax to regulate cellular responses to DNA double-strand breaks. *Cell*. 2005;123:1213-1226
65. Lu C, Zhu F, Cho YY, Tang F, Zykova T, Ma WY, Bode AM, Dong Z. Cell apoptosis: Requirement of h2ax in DNA ladder formation, but not for the activation of caspase-3. *Molecular cell*. 2006;23:121-132
66. Pignoni F, Hu B, Zavitz KH, Xiao J, Garrity PA, Zipursky SL. The eye-specification proteins so and eya form a complex and regulate multiple steps in drosophila eye development. *Cell*. 1997;91:881-891
67. Zhu S, Paydar M, Wang F, Li Y, Wang L, Barrette B, Bessho T, Kwok BH, Peng A. Kinesin kif2c in regulation of DNA double strand break dynamics and repair. *eLife*. 2020;9
68. Aguilar-Quesada R, Munoz-Gamez JA, Martin-Oliva D, Peralta A, Valenzuela MT, Matinez-Romero R, Quiles-Perez R, Menissier-de Murcia J, de Murcia G, Ruiz de Almodovar M, Oliver FJ. Interaction between atm and parp-1 in response to DNA damage and sensitization of atm deficient cells through parp inhibition. *BMC Mol Biol*. 2007;8:29
69. Bartoli-Leonard F, Wilkinson FL, Schiro A, Inglott FS, Alexander MY, Weston R. Loss of sirt1 in diabetes accelerates DNA damage induced vascular calcification. *Cardiovascular research*. 2020
70. Nadlonek NA, Weyant MJ, Yu JA, Cleveland JC, Jr., Reece TB, Meng X, Fullerton DA. Radiation induces osteogenesis in human aortic valve interstitial cells. *The Journal of thoracic and cardiovascular surgery*. 2012;144:1466-1470
71. Rosina M, Langone F, Giuliani G, Cerquone Perpetuini A, Reggio A, Calderone A, Fuoco C, Castagnoli L, Gargioli C, Cesareni G. Osteogenic differentiation of skeletal muscle progenitor cells is activated by the DNA damage response. *Scientific reports*. 2019;9:5447

Highlights

- DNA damage accelerates calcification of VSMCs and this is dependent on Runx2.
- DNA damage induces PARylation of Runx2 and this requires both ATM and PARP activity.
- PARylation of Runx2 results in its accumulation and subsequent increase in expression of osteogenic target genes, as well as localisation to sites of DNA damage.
- At DNA lesions, Runx2 plays a direct role in the DDR by promoting retention of pY142-H2AX and promoting apoptosis in favour of DNA repair.
- Osteogenic transition and apoptosis of VSMCs work in concert to drive vascular calcification during ageing.

Figure 1

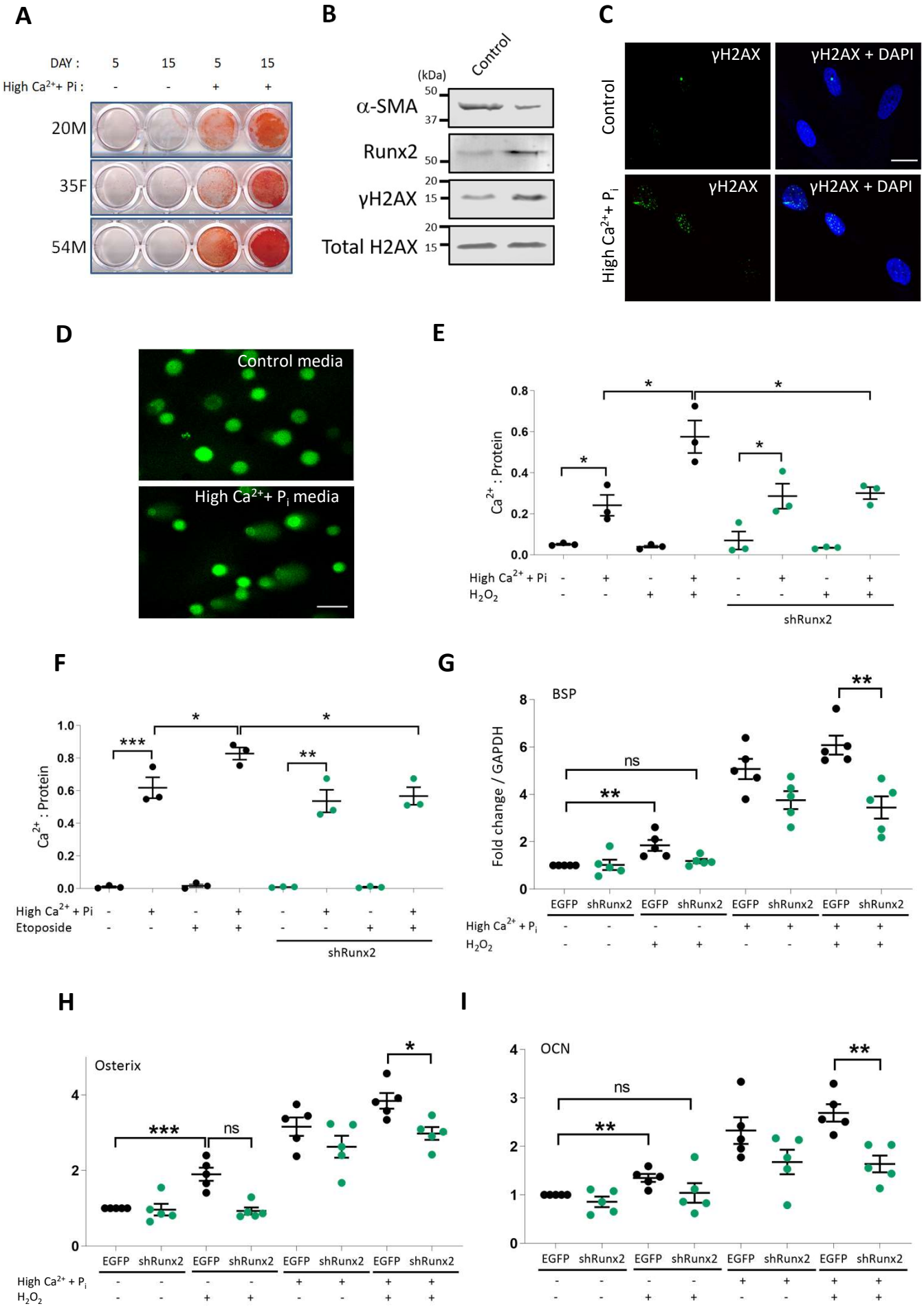
A
DAY : 5 15 5 15
High Ca2+ + Pi : - - + +
20M
35F
54M
B
Control
(kDa)
α-SMA
Runx2
γH2AX
Total H2AX
50
37
50
20
15
20
15
C
γH2AX
γH2AX + DAPI
Control
High Ca2+ + Pi
D
Control media
High Ca2+ + Pi media
E
Ca2+ : Protein
High Ca2+ + Pi
H2O2
shRunx2
F
Ca2+ : Protein
High Ca2+ + Pi
Etoposide
shRunx2
G
BSP
Fold change / GAPDH
EGFP shRunx2 EGFP shRunx2 EGFP shRunx2 EGFP shRunx2
High Ca2+ + Pi
H2O2
H
Osterix
EGFP shRunx2 EGFP shRunx2 EGFP shRunx2 EGFP shRunx2
High Ca2+ + Pi
H2O2
I
OCN
EGFP shRunx2 EGFP shRunx2 EGFP shRunx2 EGFP shRunx2

Fig. 1. **DNA damage augments VSMC calcification in a Runx2-dependent manner** (**A**) Alizarin red staining of three human VSMC isolates grown in control or calcifying media for 5 or 15 days (**B**) Western blot (WB) of protein lysate from VSMCs grown in control or calcifying media for 10 days (n = 3 (35F isolate). (**C**) Representative immunofluorescence (IF) of γH2AX in 35F VSMCs grown in control or calcifying media (10 days), DAPI is shown (blue), scale bar is 20 µm. (**D**) Representative comet assay, scale bar is 40 µm. (**E-F**) o-Cresolphthalein assay analysis showing calcification of 35F VSMCs depleted of Runx2 (shRunx2) and cultured in calcifying media, H_2O_2, etoposide or combination treatment. Treatments were for 8-12 days (n = 3). (**G-I**) RT-qPCR analysis of gene expression changes of Runx2 target genes *IBSP* (BSP), *Sp7* (Osterix) and *BGLAP* (OCN) in 35F VSMCs treated with EGFP (control) or shRunx2 that were grown in control or calcifying media and with or without H_2O_2 treatment for 9-14 days. GAPDH was used as control gene (n = 5).

Figure 2

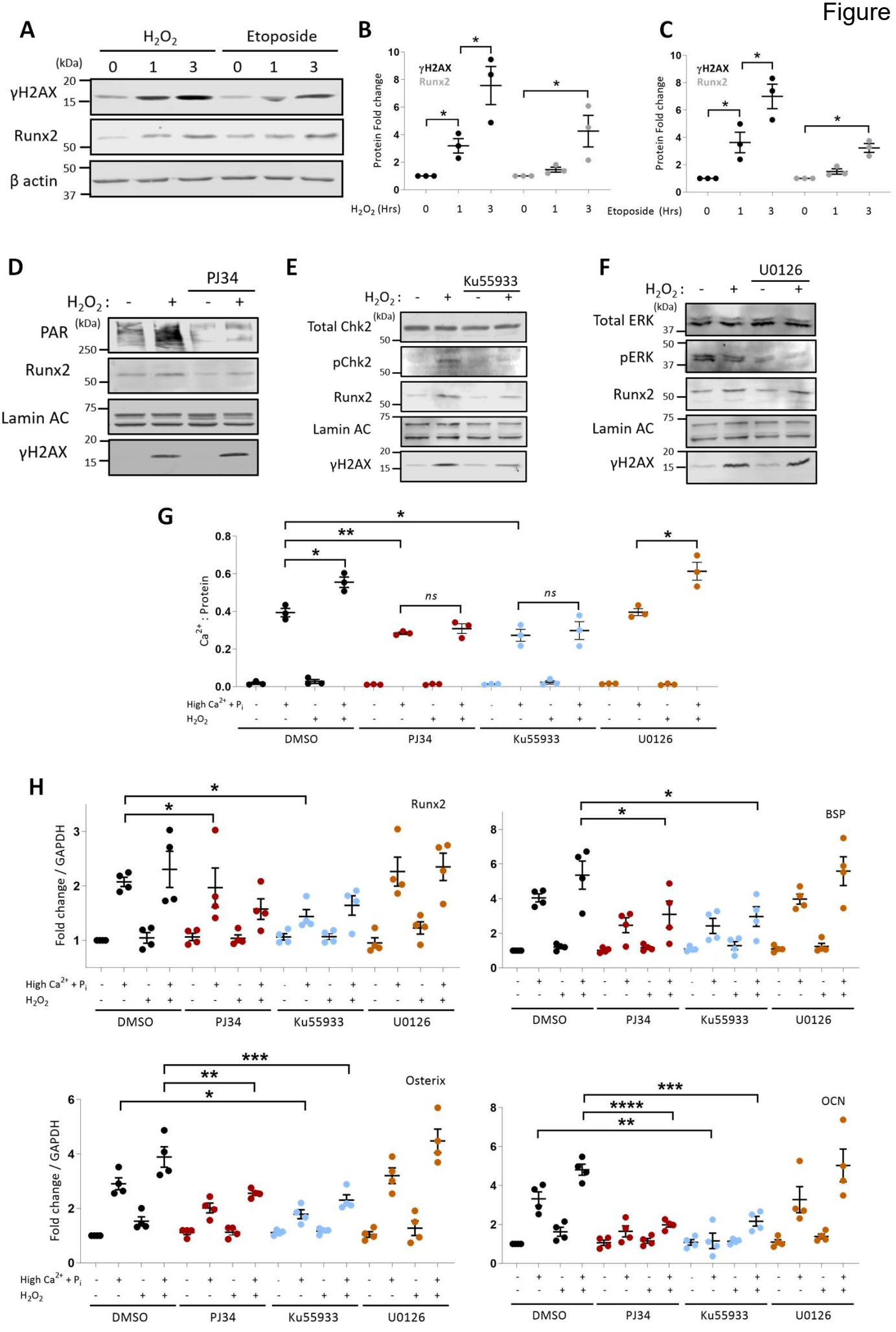
A
H2O2
Etoposide
(kDa)
0 1 3 0 1 3
γH2AX
Runx2
β actin
B
γH2AX
Runx2
Protein Fold change
H2O2 (Hrs) 0 1 3 0 1 3
C
γH2AX
Runx2
Protein Fold change
Etoposide (Hrs) 0 1 3 0 1 3
D
PJ34
H2O2 : - + - +
PAR
Runx2
Lamin AC
γH2AX
E
Ku55933
H2O2 : - + - +
Total Chk2
pChk2
Runx2
Lamin AC
γH2AX
F
U0126
H2O2 : - + - +
Total ERK
pERK
Runx2
Lamin AC
γH2AX
G
Ca2+ : Protein
High Ca2+ + Pi
H2O2
DMSO
PJ34
Ku55933
U0126
ns
H
Runx2
BSP
Osterix
OCN
Fold change / GAPDH
High Ca2+ + Pi
H2O2
DMSO
PJ34
Ku55933
U0126

Fig. 2. **DNA damage-dependent Runx2 accumulation, VSMC calcification and osteogenic gene expression are reduced by PARP and ATM inhibitors** (**A**) WB demonstrating Runx2 and γH2AX increases in 35F VSMCs treated with H_2O_2 or etoposide and (**B**-**C**) Quantification relative to β actin (n = 3). (**D**-**F**) WBs showing PJ34 and Ku55933 suppress H_2O_2 (3 hour treatment) dependent Runx2 accumulation in 35F VSMCs but U0126 does not (n = minimum of 3). (**G**) o-Cresolphthalein assay analysis showing 35F VSMC calcification following culture in calcifying media and H_2O_2 treatment (8-10 days) with additional PARP (PJ34), ATM (Ku55933) or ERK (U0126) inhibition (n = 3). (**H**) RT-qPCR analysis investigating the effect of PARP, ATM and ERK inhibition on *Runx2* (Runx2), *IBSP* (BSP), *Sp7* (Osterix) and *BGLAP* (OCN) gene expression in 35F VSMCs grown in control or calcifying media and treated with H_2O_2. Treatments were for 8-11 days. DMSO was used as a negative control (n = 3).

Figure 3

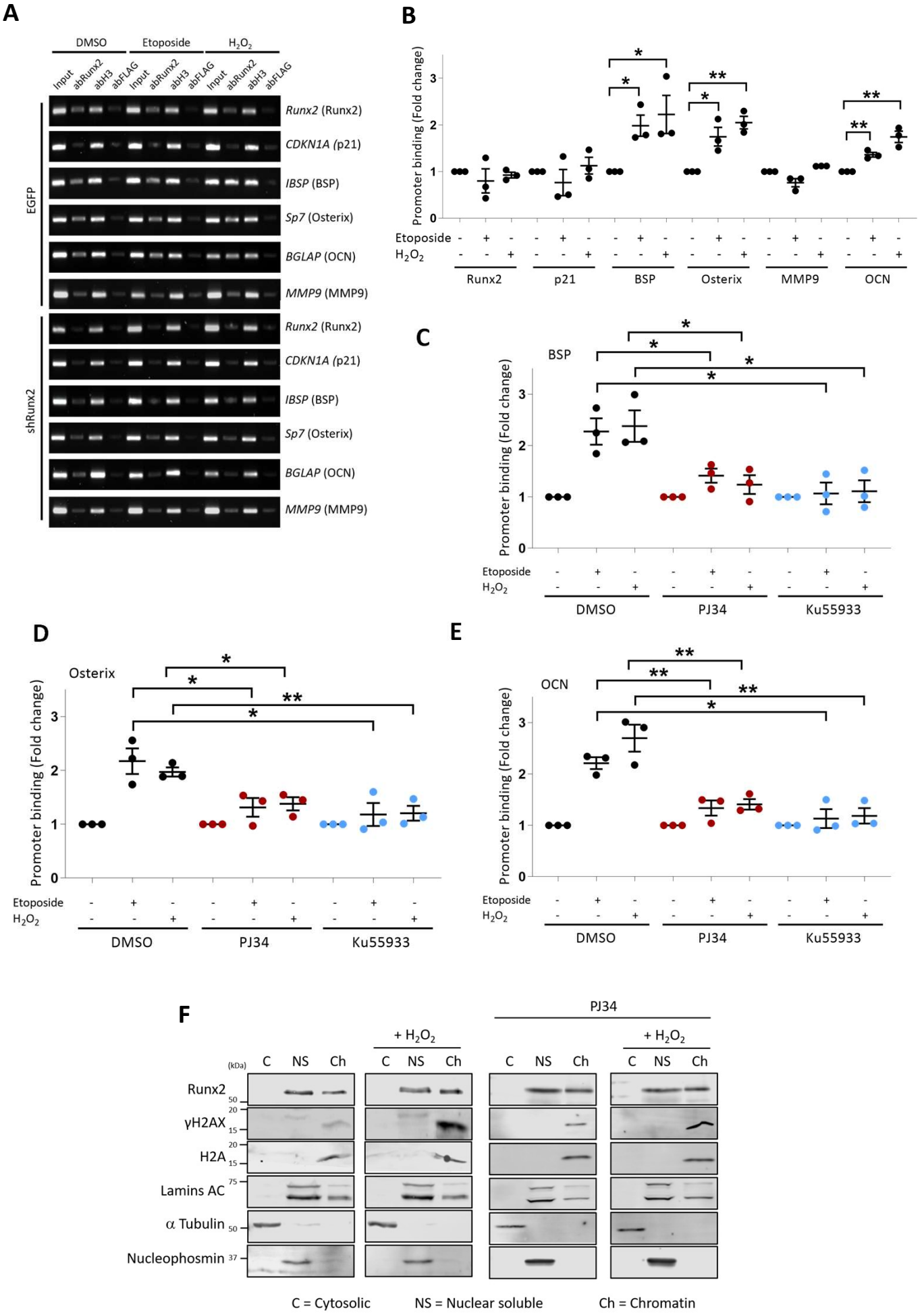
A
DMSO
Etoposide
H2O2
Input
abRunx2
abH3
abFLAG
EGFP
shRunx2
Runx2 (Runx2)
CDKN1A (p21)
IBSP (BSP)
Sp7 (Osterix)
BGLAP (OCN)
MMP9 (MMP9)
B
Promoter binding (Fold change)
Etoposide
H2O2
Runx2
p21
BSP
Osterix
MMP9
OCN
C
BSP
Promoter binding (Fold change)
Etoposide
H2O2
DMSO
PJ34
Ku55933
D
Osterix
Promoter binding (Fold change)
Etoposide
H2O2
DMSO
PJ34
Ku55933
E
OCN
Promoter binding (Fold change)
Etoposide
H2O2
DMSO
PJ34
Ku55933
F
PJ34
+ H2O2
C
NS
Ch
(kDa)
Runx2
γH2AX
H2A
Lamins AC
α Tubulin
Nucleophosmin
C = Cytosolic
NS = Nuclear soluble
Ch = Chromatin

Fig. 3. **The DDR causes enhanced Runx2 binding to osteogenic target gene promoters and changes in nuclear compartmentalization.** (**A**) PCR analysis of Runx2 target promoter chromatin immunoprecipitation (ChIP) assays performed in control (EGFP) or shRunx2 treated 35F VSMCs that were further treated with DMSO, etoposide or H_2O_2 for 8 days. Anti-Runx2 (abRunx2) (D130-3) was used to precipitate Runx2 and bound chromatin. abH3 was a positive control and abFLAG was negative control. (**B**) qPCR analysis of chromatin precipitated from control 35F VSMCs that were further treated with etoposide or H_2O_2 (5-8 days) (n = 3). (**C**-**E**) qPCR analysis from ChIP assays investigating the effect of PARP (PJ34) and ATM (Ku55933) inhibition on Runx2 binding to *IBSP* (BSP), *Sp7* (Osterix) and *BGLAP* (OCN) promoter regions in 35F VSMCs treated with etoposide or H_2O_2 for 5-10 days. DMSO was used as a no inhibitor control (n = 3). (**F**) WB of biochemical fractionation of 35F VSMCs following 3 hour H_2O_2 treatment with or without PJ34. Cells were fractioned into cytosolic, nuclear soluble and chromatin fractions.

Figure 4

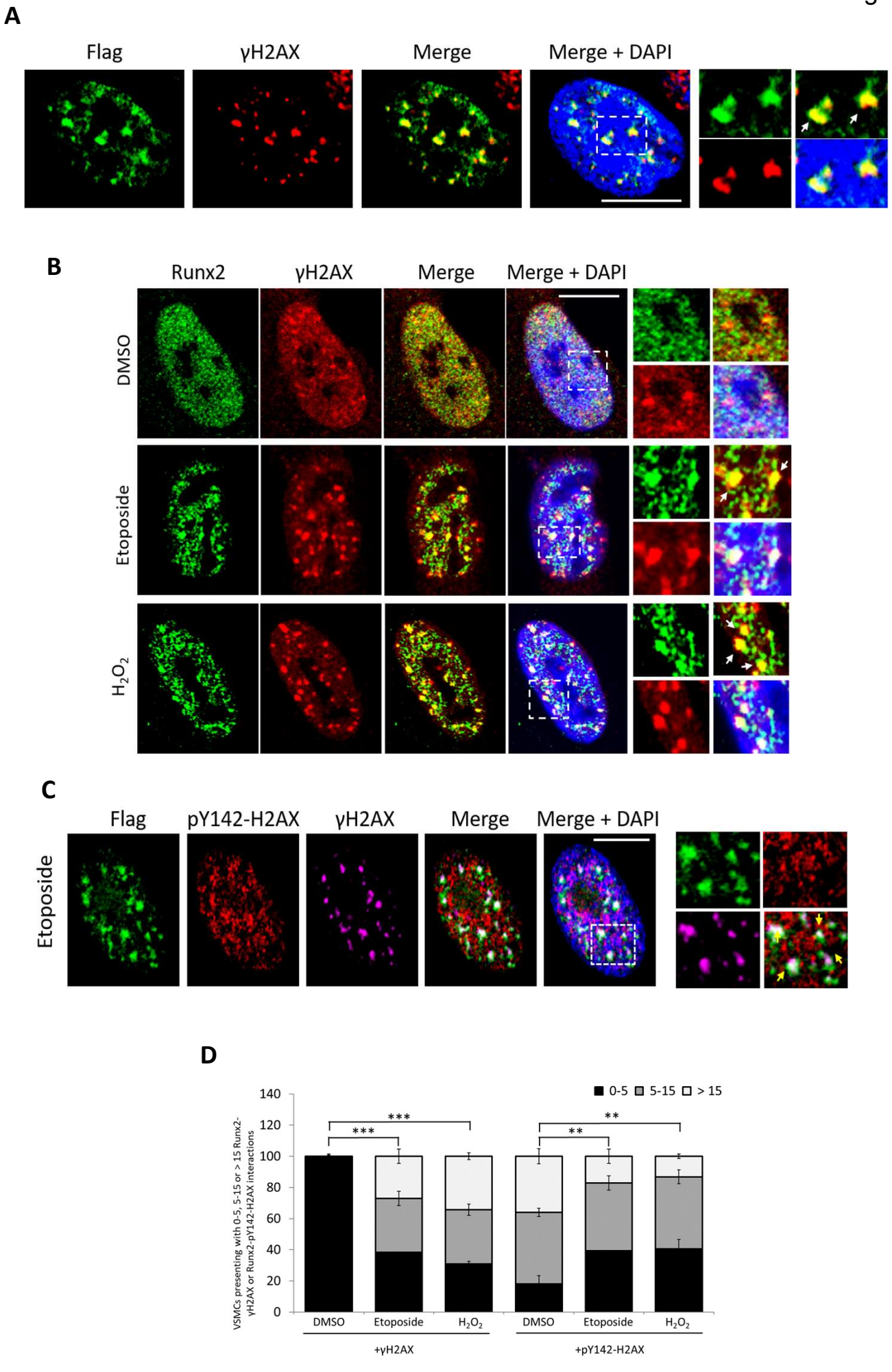
A
Flag
γH2AX
Merge
Merge + DAPI
B
Runx2
γH2AX
Merge
Merge + DAPI
DMSO
Etoposide
H2O2
C
Flag
pY142-H2AX
γH2AX
Merge
Merge + DAPI
Etoposide
D
0-5
5-15
> 15
VSMCs presenting with 0-5, 5-15 or > 15 Runx2-γH2AX or Runx2-pY142-H2AX interactions
140
120
100
80
60
40
20
0
***
***
**
**
DMSO
Etoposide
H2O2
DMSO
Etoposide
H2O2
+γH2AX
+pY142-H2AX

Fig. 4. **Runx2 forms distinct nucleoplasmic structures that are spatially associated with γH2AX and pY142-H2AX** (**A**) IF showing FL-Runx2 (Flag) and γH2AX in 35F VSMCs treated with H_2O_2 (3 hours). White arrows indicate colocalisation. DNA is stained with DAPI (blue). Scale bar is 10 μm. (**B**) IF showing endogenous Runx2 and γH2AX in 35F VSMCs treated with DMSO, etoposide or H_2O_2 (3 hours). DNA is stained with DAPI (blue). White arrows indicate colocalisation. Scale bar is 10 μm. (**C**) Triple staining IF image showing FL-Runx2, pY142-H2AX and γH2AX in a 35F VSMC treated with etoposide (3 hours). DNA is stained with DAPI (blue). Yellow arrows indicate colocalisation of FL-Runx2 and γH2AX in pockets devoid of pY142-H2AX. Scale bar is 10 μm. (**D**) Quantification proximity ligation assays (means from 3 independent experiments with n > 100 cells per experiment) is also shown. Cells were grouped into 0-5 (low genomic damage), 5-15 (moderate genomic damage) and > 15 foci (high genomic damage) / cell groups. Comparisons were performed on the > 15 groups.

Figure 5

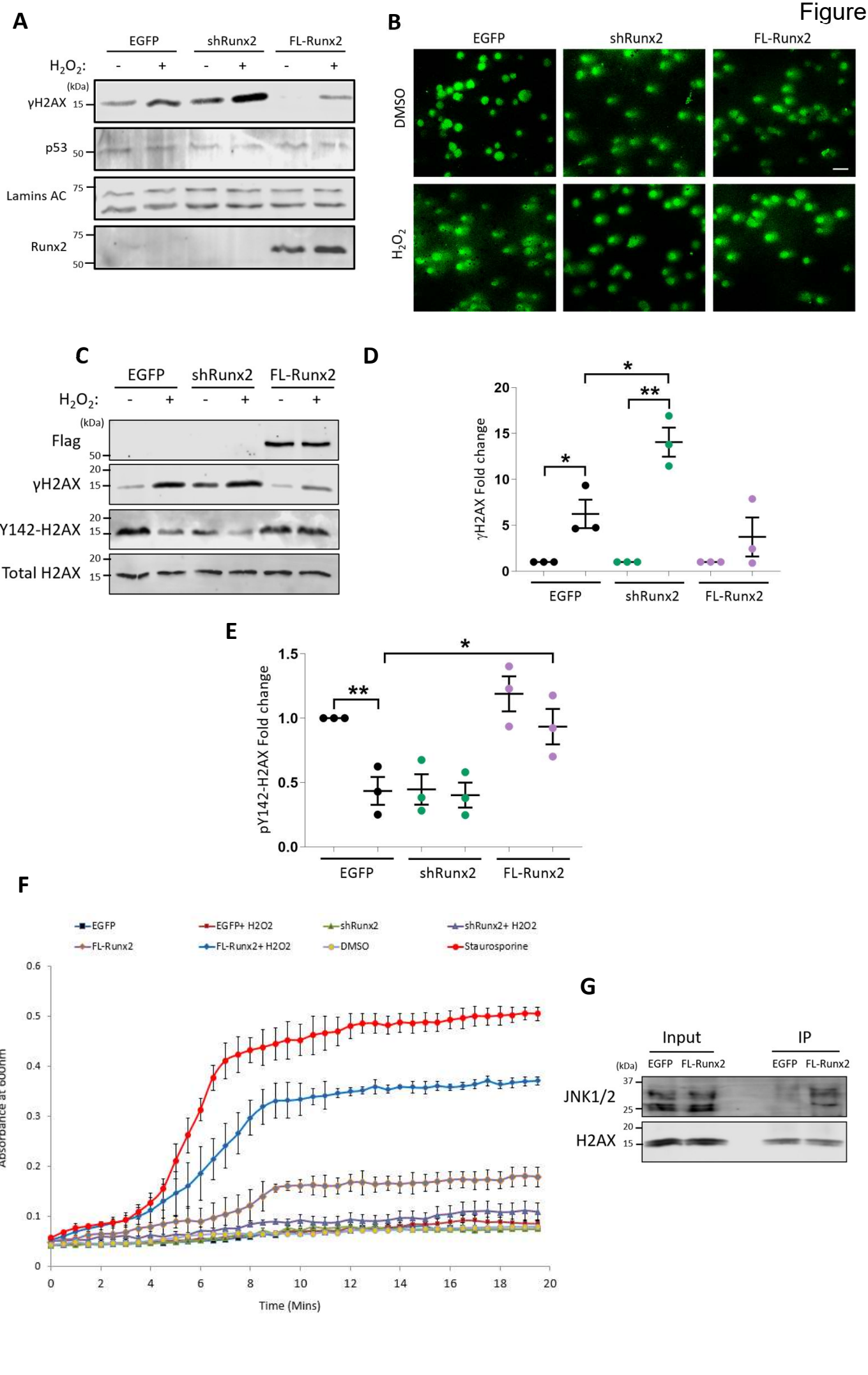
A
EGFP
shRunx2
FL-Runx2
H2O2: - + - + - +
(kDa)
γH2AX 15
p53 50
Lamins AC 75
Runx2 75 50
B
EGFP
shRunx2
FL-Runx2
DMSO
H2O2
C
EGFP
shRunx2
FL-Runx2
H2O2: - + - + - +
(kDa)
Flag 50
γH2AX 20 15
pY142-H2AX 20 15
Total H2AX 20 15
D
γH2AX Fold change
20
15
10
5
0
*
**
*
EGFP
shRunx2
FL-Runx2
E
pY142-H2AX Fold change
1.5
1.0
0.5
0.0
**
*
EGFP
shRunx2
FL-Runx2
F
EGFP
EGFP+ H2O2
shRunx2
shRunx2+ H2O2
FL-Runx2
FL-Runx2+ H2O2
DMSO
Staurosporine
Absorbance at 600nm
0.6
0.5
0.4
0.3
0.2
0.1
0
0 2 4 6 8 10 12 14 16 18 20
Time (Mins)
G
Input
IP
(kDa)
EGFP FL-Runx2
EGFP FL-Runx2
JNK1/2 37 25
H2AX 20 15

Fig. 5. **Runx2 represses γH2AX following genotoxic stress and promotes retention of pY142-H2AX causing increased VSMC apoptosis** (**A**) WB showing dysregulated γH2AX caused by Runx2 over-expression or depletion in 35F VSMCs at both baseline and after H_2O_2 (3 hour treatment). Lamins AC and p53 were unaffected by Runx2 (**B**) Representative comet assay raw data showing 35F VSMCs expressing either EGFP (control), FL-Runx2 or shRunx2 and treated for 3 hours with DMSO or H_2O_2. DNA is stained with Nancy-520. Scale bar is 40 μm. (**E**) WB of γH2AX and pY142-H2AX in 35F VSMCs expressing EGFP, shRunx2 or FL-Runx2 and treated with H_2O_2 for 3 hours. Total H2AX is shown as a control. (**F** and **G**) Quantification of band intensities of both γH2AX and pY142-H2AX from experiments shown in **E** (n = 3). (**F**) Data from active Caspase 3 ELISA. 35F VSMCs expressing EGFP, shRunx2 or FL-Runx2 were treated for 3 hours with H_2O_2 to determine sensitivity to apoptosis. Absorbance at 600 nm represents levels of cleaved Caspase 3. Staurosporine was used as a positive control for apoptosis (n = 3). (**G**) WB of co-immunoprecipitation assay investigating JNK binding to H2AX. 35F VSMCs expressing either EGFP or FL-Runx2 were treated for 3 hours with etoposide prior to using H2AX as bait to pull-down JNK. The two bands represent JNK1 and 2.

Figure 6

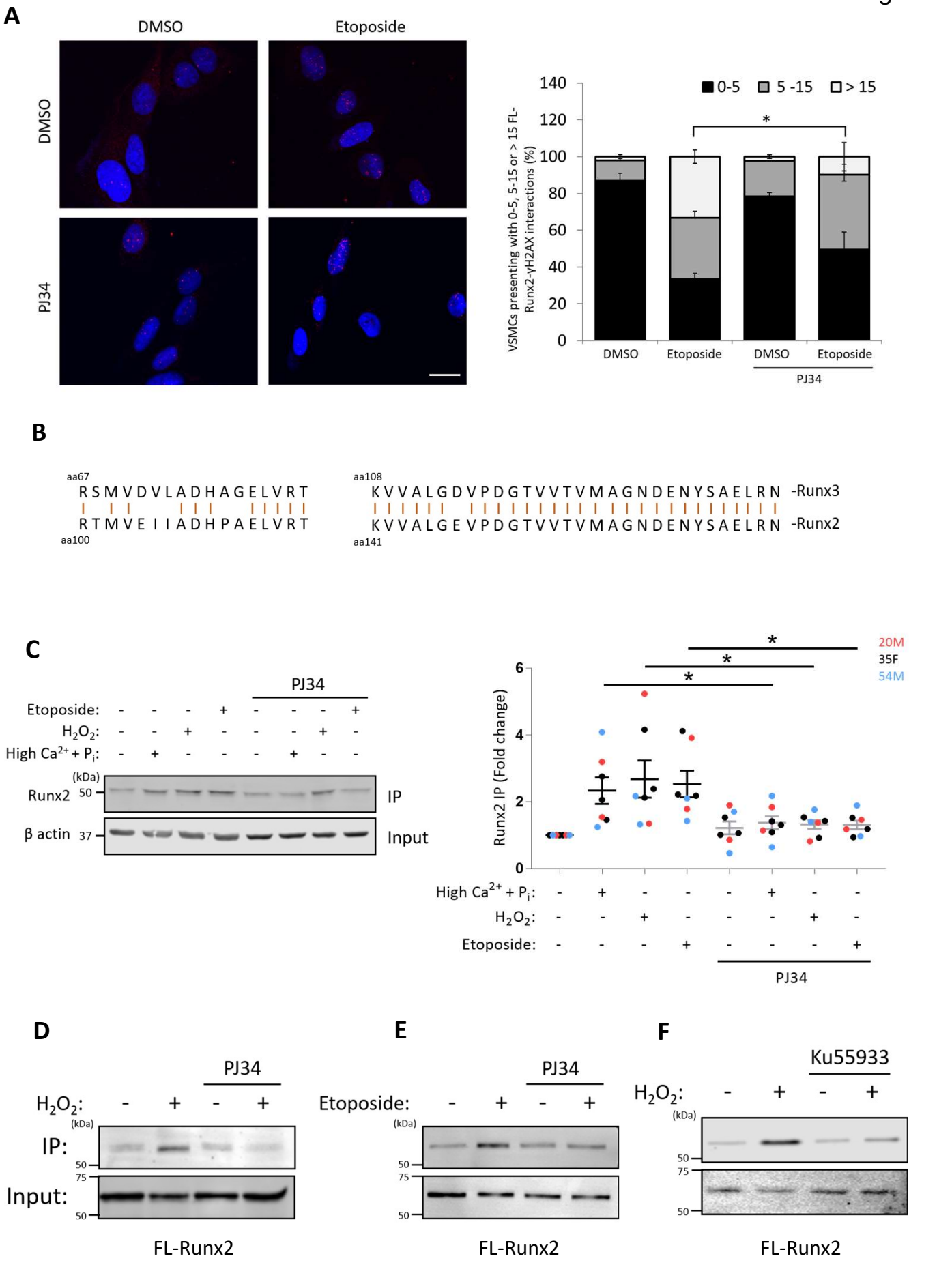
A
DMSO
Etoposide
DMSO
PJ34
0-5
5 -15
> 15
VSMCs presenting with 0-5, 5-15 or > 15 FL-Runx2-γH2AX interactions (%)
DMSO
Etoposide
DMSO
Etoposide
PJ34
B
aa67
R S M V D V L A D H A G E L V R T
R T M V E I I A D H P A E L V R T
aa100
aa108
K V V A L G D V P D G T V V T V M A G N D E N Y S A E L R N -Runx3
K V V A L G E V P D G T V V T V M A G N D E N Y S A E L R N -Runx2
aa141
C
PJ34
Etoposide:
H2O2:
High Ca2+ + Pi:
(kDa)
Runx2 50
β actin 37
IP
Input
20M
35F
54M
Runx2 IP (Fold change)
High Ca2+ + Pi:
H2O2:
Etoposide:
PJ34
D
PJ34
H2O2:
(kDa)
IP:
Input:
FL-Runx2
E
PJ34
Etoposide:
(kDa)
FL-Runx2
F
Ku55933
H2O2:
(kDa)
FL-Runx2

Fig. 6. **Runx2 is PARylated in response to genotoxic stress.** (**A**) Representative image and quantification of PLAs investigating FL-Runx2 interactions with γH2AX in 35F VSMCs treated for 3 hours with etoposide and additional PJ34 treatment (means from 3 independent experiments with n > 100 cells. Scale bar is 20 μm. Cells were grouped into 0-5 (low genomic damage), 5-15 (moderate genomic damage) and > 15 foci (high genomic damage) / cell groups. Comparisons were performed on the > 15 groups. (**B**) Amino acid sequence analysis showing hypothesised PARylated regions within Runx3 are conversed within Runx2. (**C**) WB and quantification from boronate bead pull-down assays (BBPDAs) of endogenous Runx2 from 3 VSMCs isolates treated with calcifying media, H_2O_2 or etoposide for 11-14 days. PJ34 treatment was used to assess PARP inhibition. β-actin shows lysate input. For quantification, fold change of Runx2 was normalised to β-actin input (n = 7). (**D**) WB from BBPDAs of FL-Runx2 expressed in 35F VSMCs treated with or without H_2O_2 and PJ34 PARP inhibitor (3 hour treatments) (n = 4). (**E**) WB from BBPDAs of FL-Runx2 expressed in 35F VSMCs treated with or without etoposide and PJ34 PARP inhibitor (3 hour treatments) (n = 5). (**F**) Representative WB from BBPDAs of FL-Runx2 expressed in 35F VSMCs treated with or without H_2O_2 and Ku55933 ATM inhibitor (3 hour treatments) (n = 4).

Figure 7

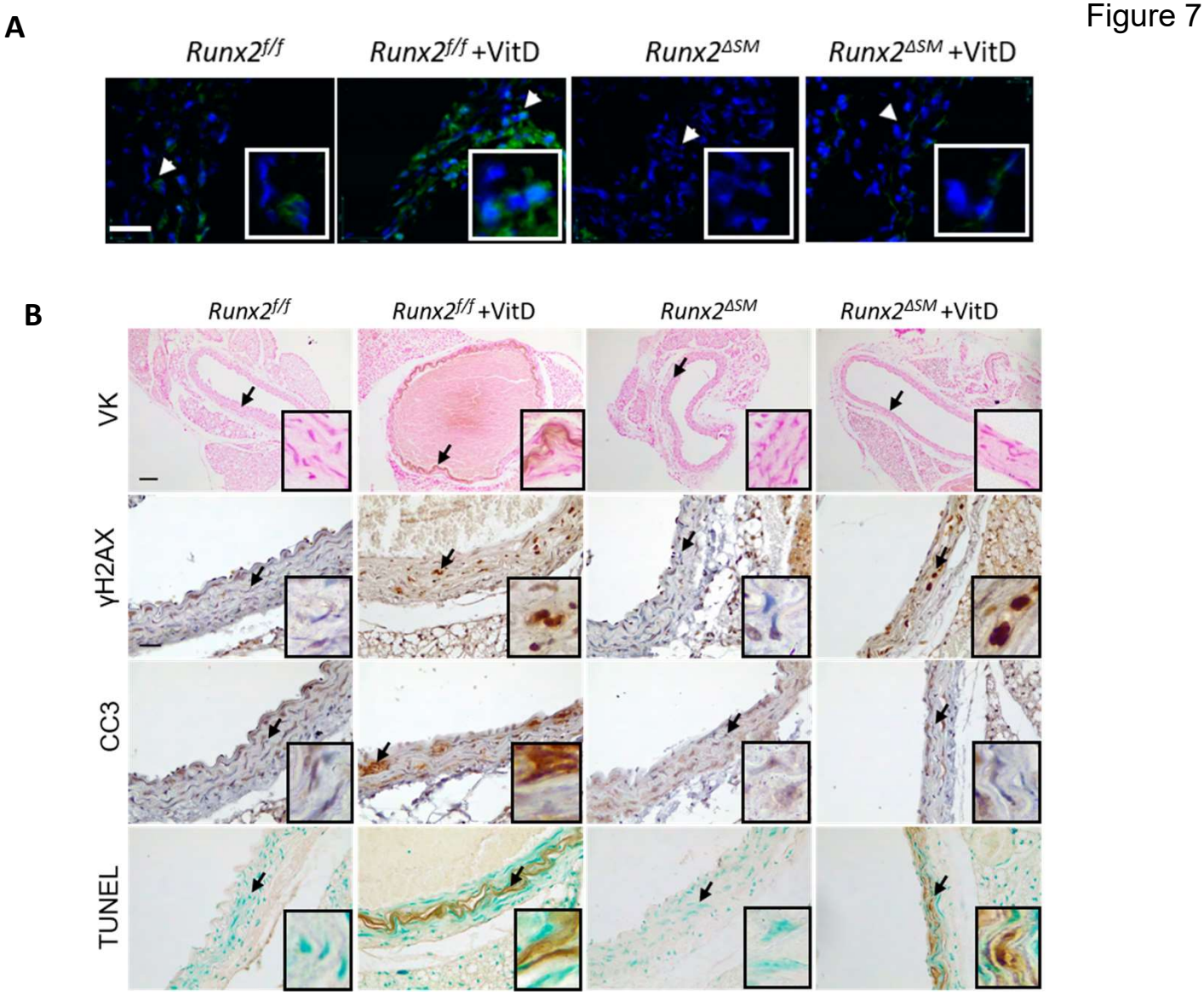
A
Runx2f/f
Runx2f/f +VitD
Runx2ΔSM
Runx2ΔSM +VitD
B
Runx2f/f
Runx2f/f +VitD
Runx2ΔSM
Runx2ΔSM +VitD
VK
γH2AX
CC3
TUNEL
C
Runx2 gene expression / GAPDH
D
BSP gene expression / GAPDH
E
Osterix gene expression / GAPDH
VitD:
F
OCN gene expression / GAPDH
G
Runx2f/f
Runx2ΔSM
VitD:
(kDa)
Runx2
IP
β actin
Input
Runx2 IP (Fold change)
ns

Fig. 7. **Runx2 localizes with γH2AX in calcified arteries, is essential for osteogenic gene expression and is PARylated in response to vitamin D treatment *in vivo.*** (**A**) IF of Runx2 staining (green) in control (*Runx2*$^{f/f}$) and smooth muscle-specific Runx2 knock-out (*Runx2*$^{\Delta SM}$)mice aortas treated with or without vitamin D (VitD). White arrows show enlarged area, scale bar is 30 μm. (**B**) Immunohistochemistry of aorta from the same mice stained for von Kossa (calcified regions), γH2AX (DNA damage), CC3 (cleaved caspase-3 (apoptosis)) and TUNEL staining (fragmented DNA (**C-F**) RT-qPCR of *Runx2* (Runx2), *IBSP (*BSP), *Sp7* (Osterix) and *BGLAP* (OCN) in *Runx2*$^{f/f}$ and *Runx2*$^{\Delta SM}$ mice aorta treated with or without VitD (n = 5). (**G**) BBPDA data showing PARylation of Runx2 in *Runx2*$^{f/f}$ and *Runx2*$^{\Delta SM}$ mice aorta. Representative WB (left) and quantification (right) is shown (n = 5).

Supplemental materials

Runx2 links the DNA damage response to osteogenic reprogramming and apoptosis of vascular smooth muscle cells

Andrew M. Cobb[1], Syabira Yusoff[1], Robert Hayward[1], Sadia Ahmad[1], Mengxi Sun[1], Anja Verhulst[2], Patrick C. D'Haese[2] and Catherine M. Shanahan[1]*

[1]BHF Centre of Research Excellence, School of Cardiovascular Medicine and Sciences, King's College London, The James Black Centre, 125 Coldharbour Lane, London SE5 9NU, United Kingdom.

[2]Laboratory of Pathophysiology, Department of Biomedical Sciences, University of Antwerp, Universiteitsplein 1, 2610 Wilrijk, Belgium

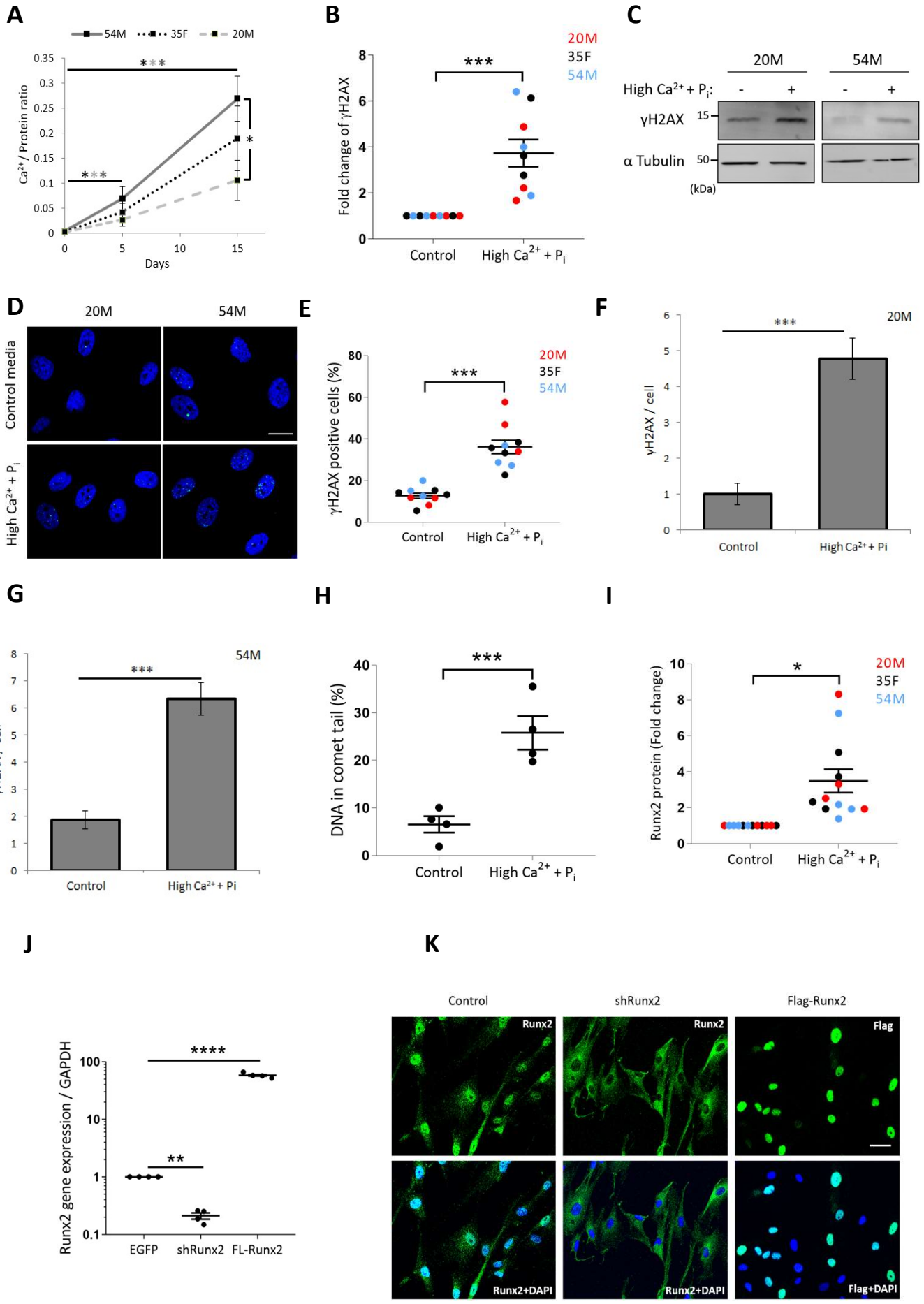
A
54M
35F
20M
Ca2+ / Protein ratio
Days
B
20M
35F
54M
Fold change of γH2AX
Control
High Ca2+ + Pi
C
20M
54M
High Ca2+ + Pi:
γH2AX
α Tubulin
(kDa)
D
20M
54M
Control media
High Ca2+ + Pi
E
γH2AX positive cells (%)
F
γH2AX / cell
G
γH2AX / cell
H
DNA in comet tail (%)
I
Runx2 protein (Fold change)
J
Runx2 gene expression / GAPDH
EGFP
shRunx2
FL-Runx2
K
Control
shRunx2
Flag-Runx2
Runx2
Flag
Runx2+DAPI
Flag+DAPI

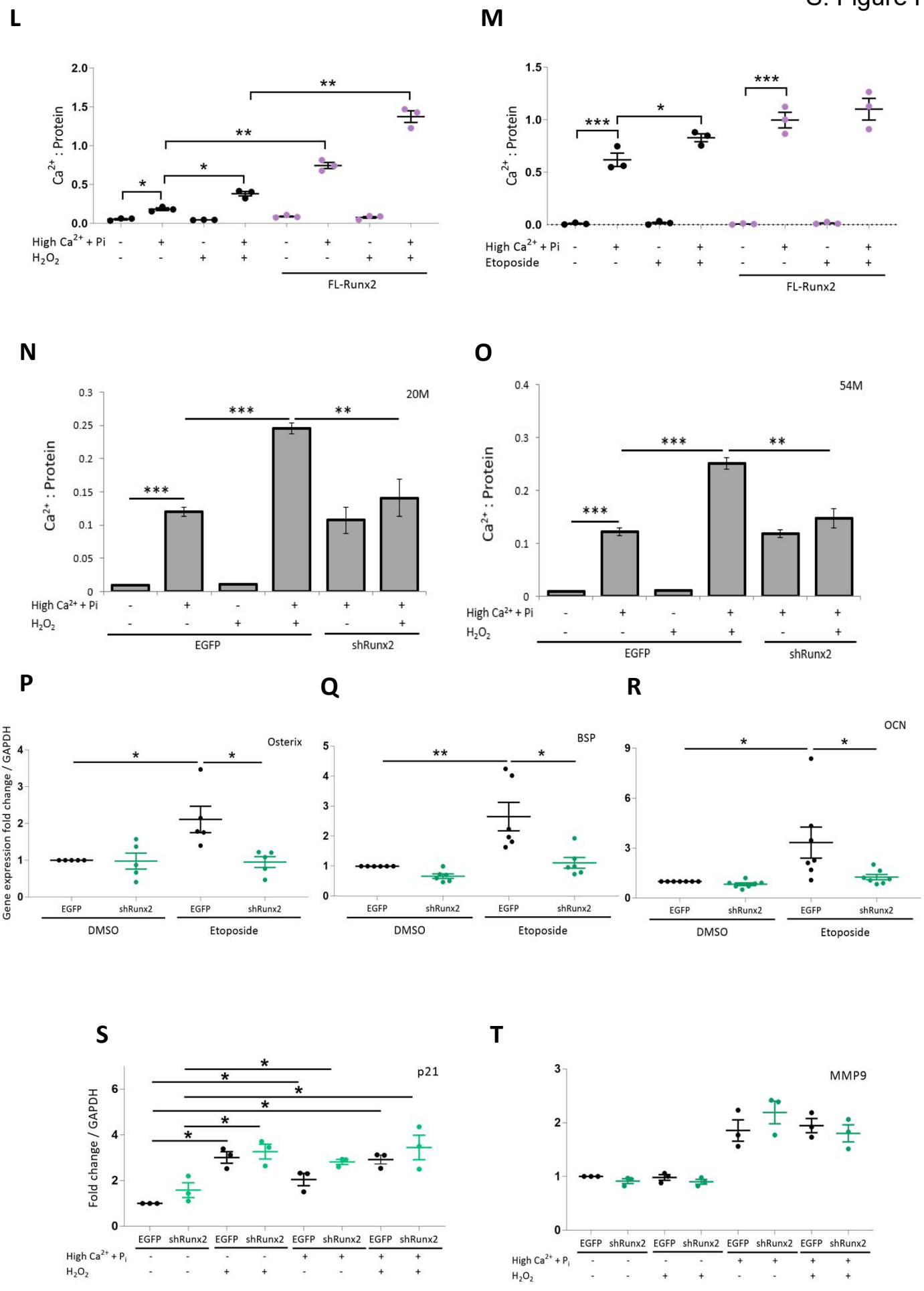
L
M
N
O
P
Q
R
S
T
Ca2+ : Protein
High Ca2+ + Pi
H2O2
Etoposide
FL-Runx2
20M
54M
EGFP
shRunx2
Gene expression fold change / GAPDH
Osterix
BSP
OCN
DMSO
Etoposide
p21
MMP9
Fold change / GAPDH

Supplementary Fig. I. **DNA damage augments VSMC calcification in a Runx2-dependent manner** (**A**) o-Cresolphthalein data of VSMCs from 3 isolates grown in calcifying media for 0-15 days (n = 3 per isolate). (**B**) Quantification of γH2AX levels in 3 VSMC isolates grown in control or calcifying media for 10-15 days (n = 9). (**C**) WB showing levels of γH2AX in 20M and 54M VSMCs cultured in normal or calcifying media for 12 days. All isolates were harvested at passage 13. α-Tubulin is used as a loading control. (**D**) IF image showing γH2AX in 20M and 54M VSMC isolates following culture in control or calcifying media for 10 days. DNA is stained with DAPI (blue). Scale bar is 20 μm. (**E**) Quantification of γH2AX foci from 3 VSMC isolates grown in the same conditions. Cells with > 5 γH2AX foci considered to have significant genetic damage (means of 3 independent experiments per isolate with n > 100 cells in each experiment). (**F** and **G**) IF quantification of γH2AX in 20M and 54M isolates grown in normal or calcifying media for 8-12 days (means of 3 independent experiments with n > 100 cells). (**H**) Comet assay quantification -35F VSMCs grown in control or calcifying media for 10-12 days. (means of 3 independent experiments with n = 100). (**I**) Quantification of Runx2 levels in 3 VSMC isolates grown in control or calcifying media for 10-15 days (n = 9). (**J**) RT-qPCR analysis of Runx2 gene expression in 35F VSMCs following short-hairpin RNA interference (shRunx2) or over-expression of recombinant FLAG-tagged Runx2 (FL-Runx2) (n = 4). (**K**) Representative IF of 35F VSMCs treated with EGFP (control), shRunx2 or FL-Runx2. Runx2 is stained green. DNA is stained with DAPI (blue). Scale bar is 40 μm.). (**L-M**) o-Cresolphthalein assay analysis showing calcification of 35F VSMCs over-expressing Runx2 (FL-Runx2) and cultured in calcifying media, H_2O_2, etoposide or combination treatment. Treatments were for 8-12 days (n = 3). (**N-O**) o-Cresolphthalein assay analysis showing 20M and 54M VSMC calcification following culture in calcifying media and treated with $H_2O_2$for 9-13 days. (n = 3). (**P-R**) RT-qPCR data showing the effect of etoposide (8-12 days) upon expression of a subset of Runx2 regulated genes *Sp7* (Osterix) (**P**), *IBSP* (BSP) (**Q**) and *BGLAP* (OCN) (**R**). Cells were expressing either EGFP or shRunx2 to assess the impact of Runx2 on expression. DMSO was used as a control (n = 5-7). (**S-T**) RT-qPCR data showing gene expression changes of Runx2 target genes *CDKN1A* (p21) and *MMP9* (MMP9) in 35F VSMCs treated with EGFP (control) or shRunx2 that were grown in control or calcifying media and with or without H_2O_2 treatment for 9-14 days. GAPDH was used as the control gene (n = 3).

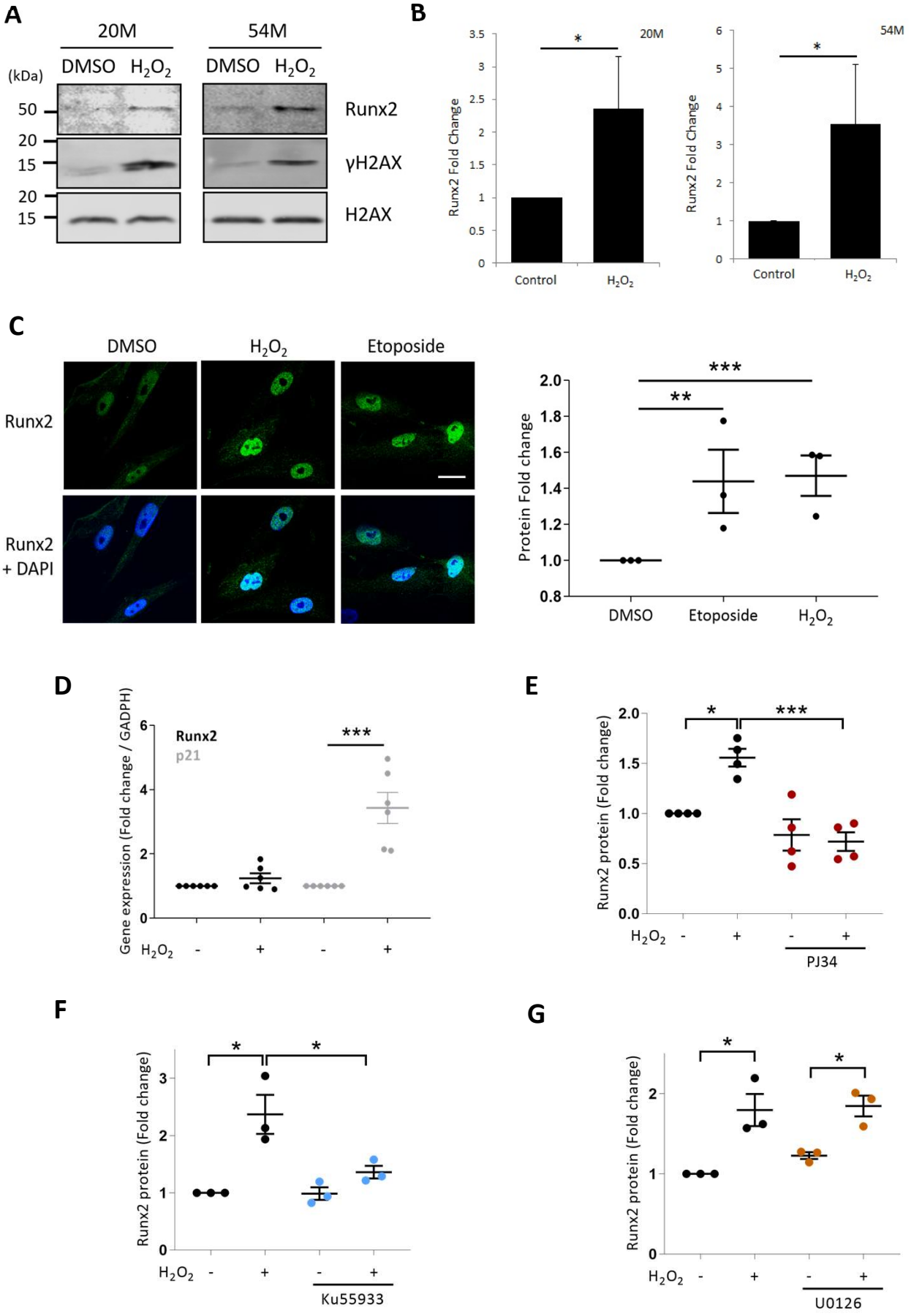
A
20M
54M
(kDa)
DMSO
H2O2
DMSO
H2O2
50
20
15
20
15
Runx2
γH2AX
H2AX
B
20M
54M
Runx2 Fold Change
Control
H2O2
C
DMSO
H2O2
Etoposide
Runx2
Runx2
+ DAPI
Protein Fold change
DMSO
Etoposide
H2O2
D
Runx2
p21
Gene expression (Fold change / GADPH)
H2O2
E
Runx2 protein (Fold change)
H2O2
PJ34
F
Runx2 protein (Fold change)
H2O2
Ku55933
G
Runx2 protein (Fold change)
H2O2
U0126

Supplementary Fig. II. **DNA damage-dependent Runx2 accumulation, VSMC calcification and osteogenic gene expression are reduced by PARP and ATM inhibitors** (**A**) Representative WBs showing increases in Runx2 and γH2AX in 20M and 54M VSMCs treated with H_2O_2 for 3 hours. (**B**) Quantification of Runx2 fold change normalised to total H2AX (n = 3). (**C**) IF representative image of Runx2 staining in 35F VSMCs treated with DMSO, H_2O_2 or etoposide for 3 hours, DNA is stained with DAPI (blue). Scale bar is 20 μm. Quantification of Runx2 intensity changes (means of 3 independent experiments with n = 156 cells). (**D**) RT-qPCR data showing *Runx2* (Runx2) and *CDKN1A* (p21) gene expression in 35F VSMCs treated with H_2O_2 for 3 hours (n = 6). (**E-G**) Quantification of WBs shown in Fig 2. D-F.

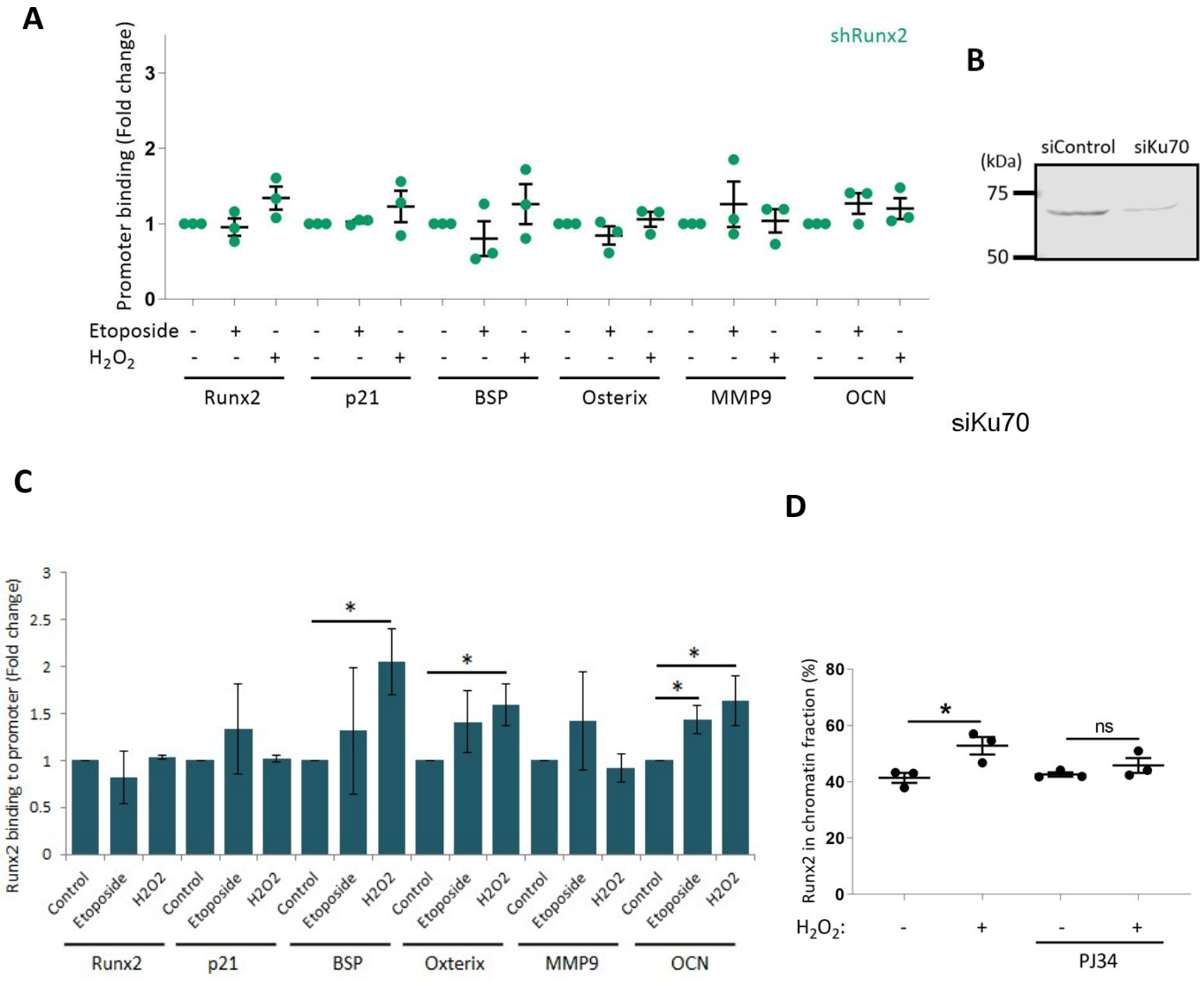

Supplementary Fig. III. **The DDR causes enhanced Runx2 binding to osteogenic target gene promoters and changes in nuclear compartmentalization.** (**A**) qPCR analysis of chromatin precipitated from shRunx2 treated 35F VSMCs that were further treated with etoposide or H_2O_2 (5-8 days) (n = 3). (**B**) Representative WB showing siRNA treatment against Ku70. (**C**) ChIP assay investigating Runx2 binding to target promoter regions in 35F VSMCs depleted of Ku70. qPCR analysis showing promoter region precipitation using anti-Runx2 antibody in 35F VSMCs treated with control (DMSO), etoposide or H_2O_2 for 8 days (n = 3). (**D**) Quantification of Runx2 localisation from biochemical fractionation experiments. Upon H_2O_2 treatment, Runx2 associated with chromatin increases by approximately 15%, however this is attenuated by PJ34 (n = 3).

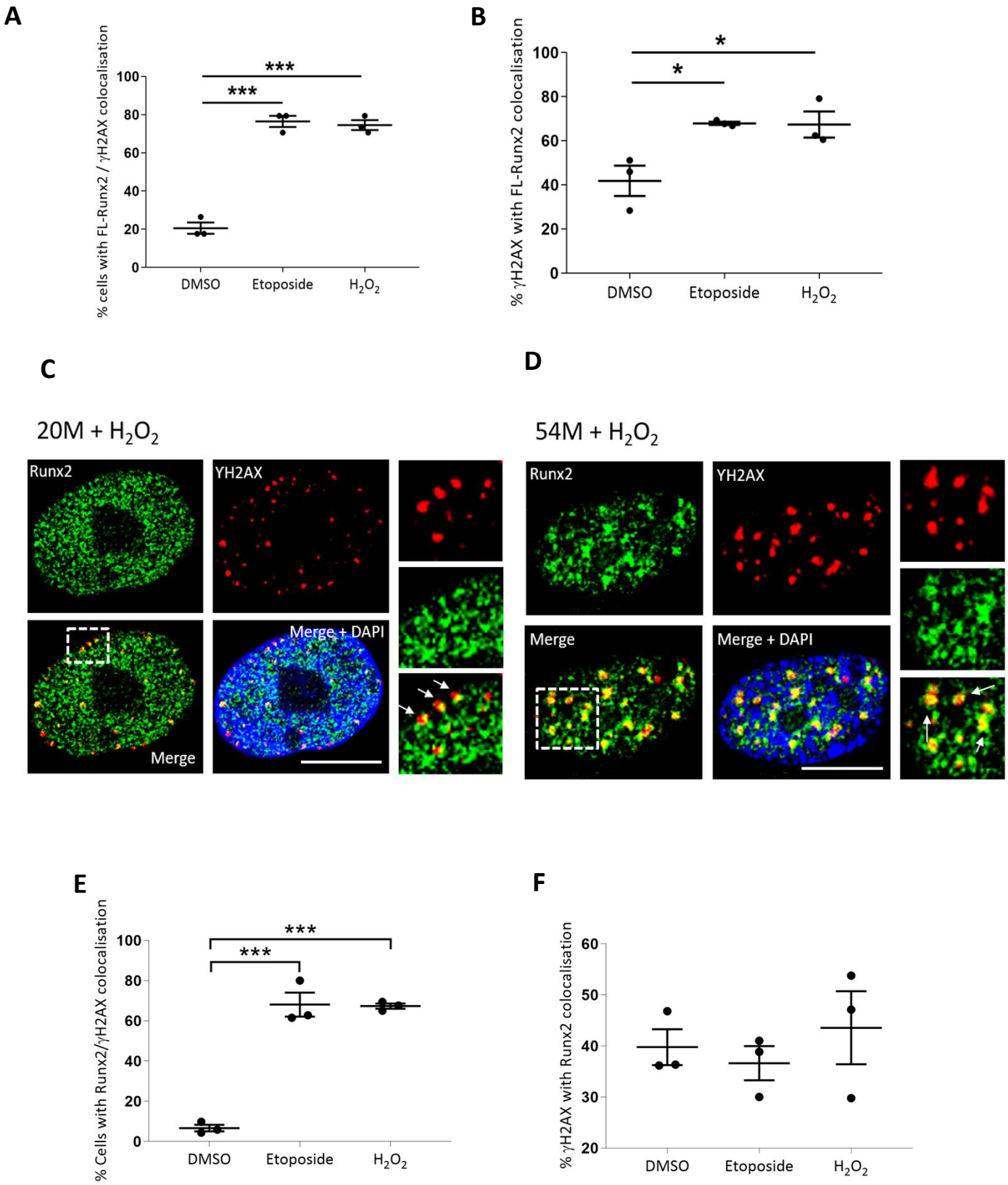
A
% cells with FL-Runx2 / γH2AX colocalisation
***
***
DMSO
Etoposide
H2O2
B
% γH2AX with FL-Runx2 colocalisation
*
*
DMSO
Etoposide
H2O2
C
20M + H2O2
Runx2
YH2AX
Merge
Merge + DAPI
D
54M + H2O2
Runx2
YH2AX
Merge
Merge + DAPI
E
% Cells with Runx2/γH2AX colocalisation
***
***
DMSO
Etoposide
H2O2
F
% γH2AX with Runx2 colocalisation
DMSO
Etoposide
H2O2

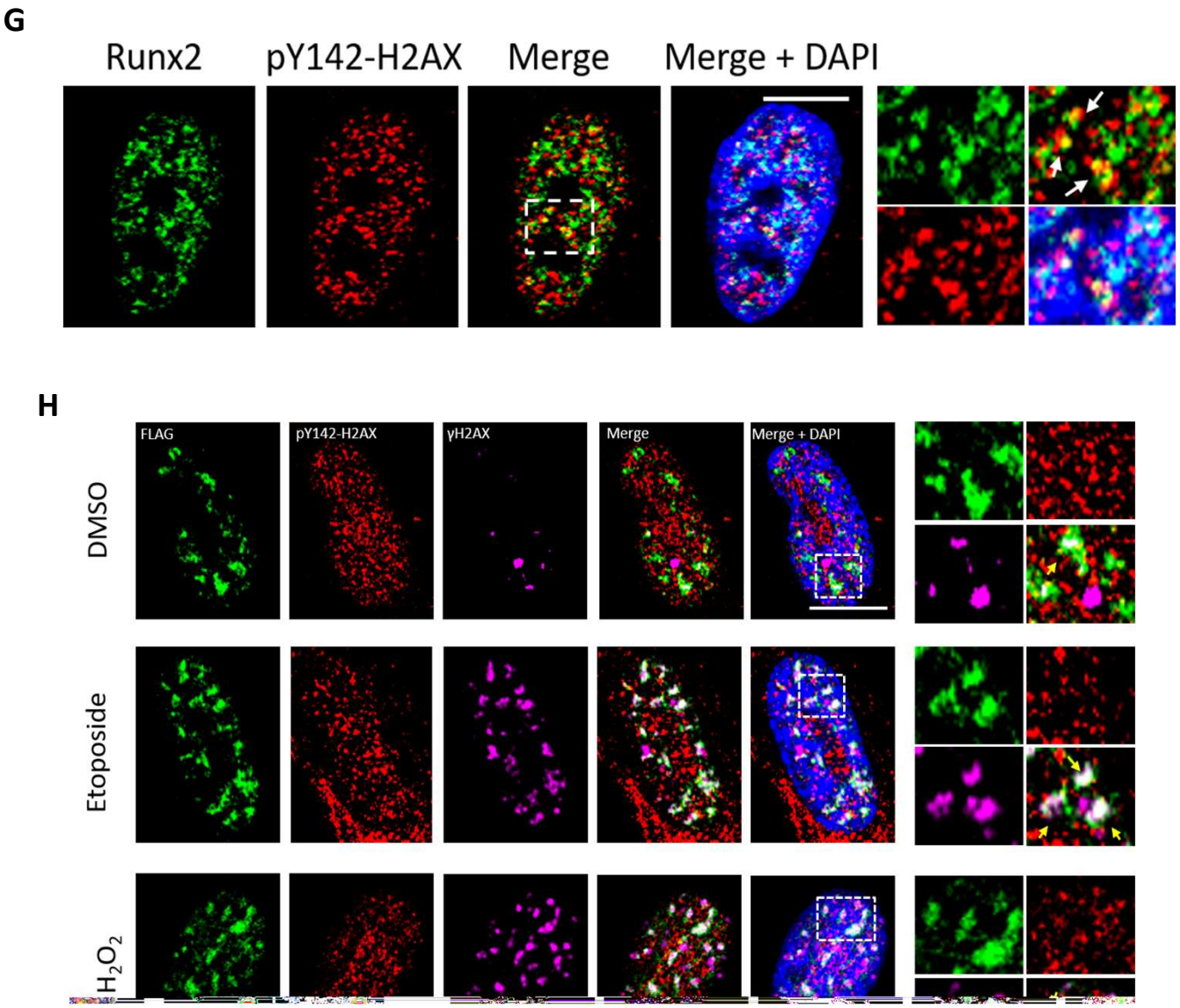
G
Runx2
pY142-H2AX
Merge
Merge + DAPI
H
FLAG
pY142-H2AX
γH2AX
Merge
Merge + DAPI
DMSO
Etoposide
H2O2
I
DMSO
H2O2
Etoposide
Ab-Runx2
Ab-Runx2+ Ab-pY142-H2AX
Ab-Runx2+ Ab-γH2AX
J
Ab-pY142-H2AX
Ab-γH2AX
Ab-Runx2
DMSO
H2O2
Etoposide

Supplementary Fig. IV. **Runx2 forms distinct nucleoplasmic structures that are spatially associated with γH2AX and pY142-H2AX** (**A** and **B**) Quantification of IF data from Fig. 4A showing percentage of 35F VSMCs that displayed FL-Runx2 and γH2AX colocalisation (**A**) and also the percentage of γH2AX that colocalised with FL-Runx2 (**B**) following 3 hour treatments of DMSO, H_2O_2 or etoposide (means from 3 independent experiments with n > 100 35F VSMCs). (**C** and **D**) IF representative image of γH2AX and endogenous Runx2 staining in 20M and 54M VSMCs following H_2O_2 treatment for 3 hours. White arrows indicate colocalisation. DNA is stained with DAPI (blue). Scale bars are 10 μm. (**E**) Quantification of IF showing percentage of cells presenting with Runx2 and γH2AX colocalisation (means from 3 independent experiments with n = 276 35F VSMCs. (**F**) IF data showing the percentage of γH2AX foci that colocalised with Runx2 (means from 3 independent experiments with n = 300 35F VSMCs. (**G**) Representative IF image showing endogenous Runx2 and pY142-H2AX in an unstressed 35F VSMC. White arrows highlight close associations between both proteins. DNA is stained with DAPI (blue). Scale bar is 10 μm. (**H**) Additional IF example showing FL-Runx2 (FLAG) forms distinct nucleoplasmic structures that are spatially associated with γH2AX and pY142-H2AX in VSMCs treated with DMSO (control) or genotoxic agents etoposide and H_2O_2 (3 hours). DNA is stained with DAPI (blue). Interactions are shown with yellow arrows. Scale bar is 10 μm. (**I**) Representative proximity ligation (PLA) image showing endogenous Runx2 interactions with γH2AX and pY142-H2AX in 35F VSMCs (red foci) treated with DMSO, etoposide or H_2O_2 (all 3-hour treatments). Scale bar is 20 μm. (**J**) Representative IF images from negative control PLAs performed in 35F VSMCs treated with DMSO, etoposide or H_2O_2 (3 hours). Only one antibody was used in each condition (no positive signal detected).

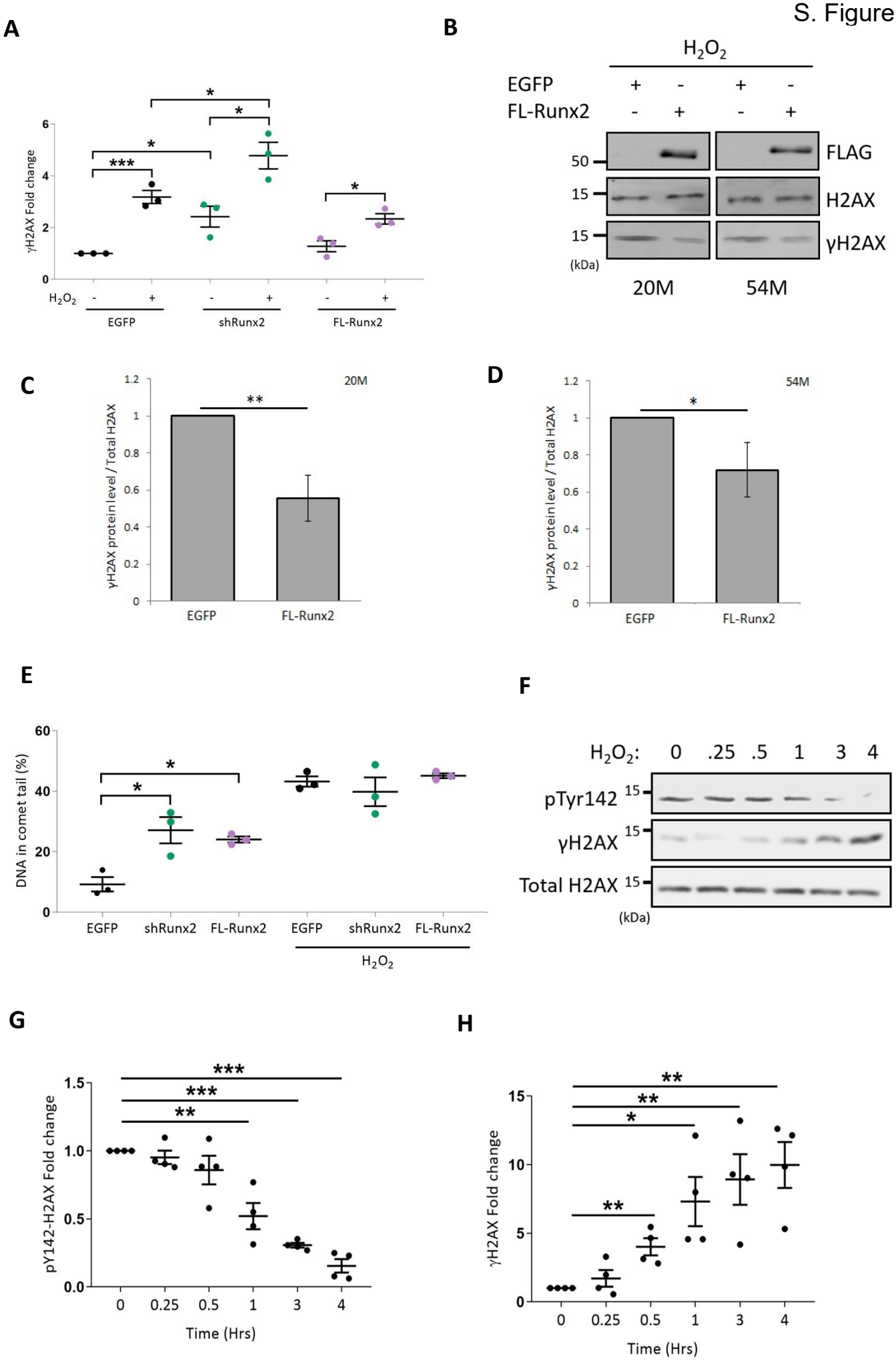
A
γH2AX Fold change
H2O2
EGFP
shRunx2
FL-Runx2
B
H2O2
EGFP
FL-Runx2
FLAG
H2AX
γH2AX
(kDa)
20M
54M
C
20M
γH2AX protein level / Total H2AX
EGFP
FL-Runx2
D
54M
γH2AX protein level / Total H2AX
EGFP
FL-Runx2
E
DNA in comet tail (%)
EGFP
shRunx2
FL-Runx2
H2O2
F
H2O2: 0 .25 .5 1 3 4
pTyr142
γH2AX
Total H2AX
(kDa)
G
pY142-H2AX Fold change
Time (Hrs)
H
γH2AX Fold change
Time (Hrs)

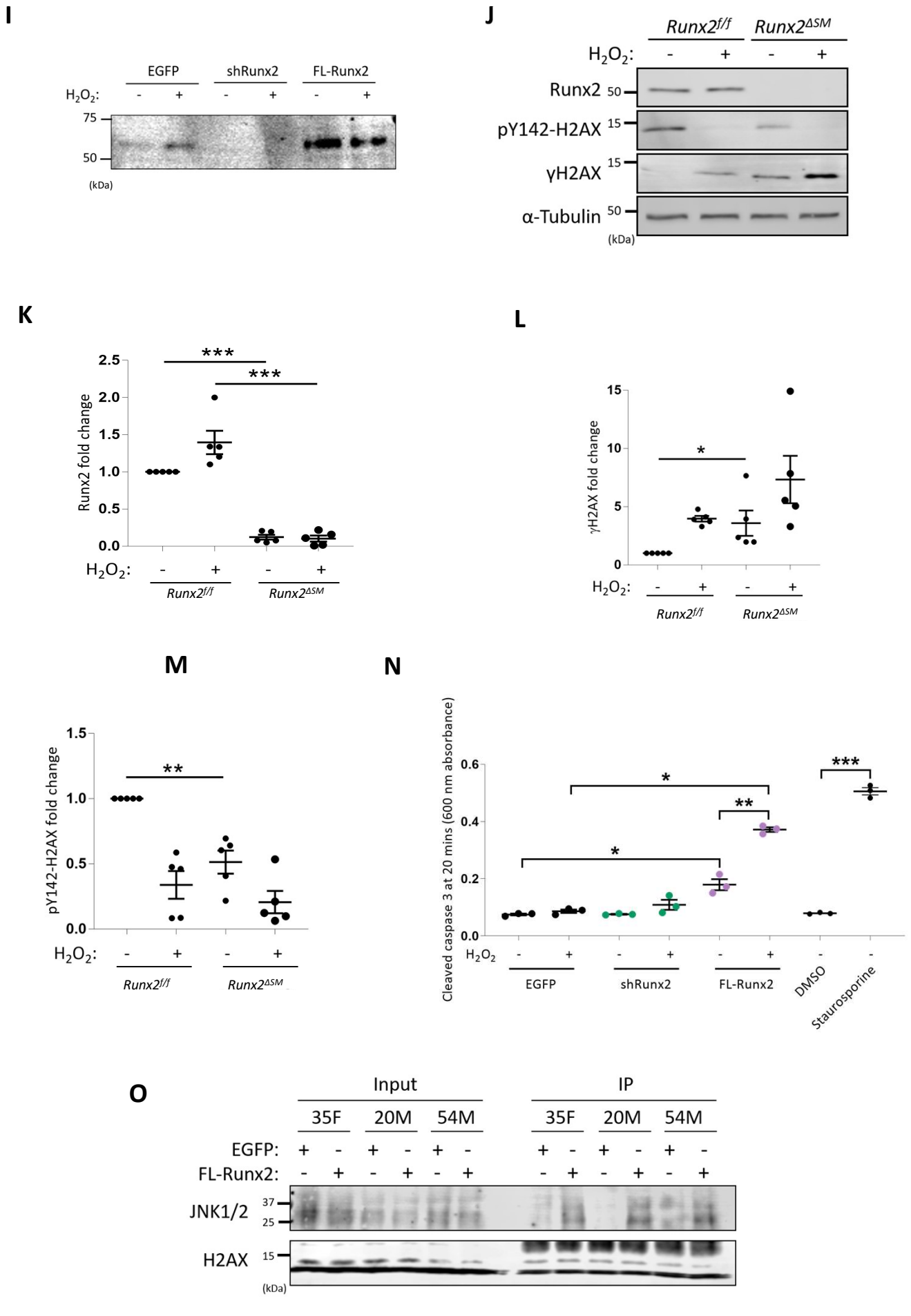
I
EGFP
shRunx2
FL-Runx2
H2O2: - + - + - +
75
50
(kDa)
J
Runx2f/f
Runx2ΔSM
H2O2: - + - +
Runx2 50
pY142-H2AX 15
γH2AX 15
α-Tubulin 50
(kDa)
K
Runx2 fold change
H2O2: - + - +
Runx2f/f
Runx2ΔSM
L
γH2AX fold change
H2O2: - + - +
Runx2f/f
Runx2ΔSM
M
pY142-H2AX fold change
H2O2: - + - +
Runx2f/f
Runx2ΔSM
N
Cleaved caspase 3 at 20 mins (600 nm absorbance)
H2O2 - + - + - + - -
EGFP
shRunx2
FL-Runx2
DMSO
Staurosporine
O
Input
IP
35F 20M 54M 35F 20M 54M
EGFP: + - + - + - + - + - + -
FL-Runx2: - + - + - + - + - + - +
JNK1/2 37 25
H2AX 15
(kDa)

Supplementary Fig. V. **Runx2 represses γH2AX following genotoxic stress and promotes retention of pY142-H2AX causing increased VSMC apoptosis** (**A**) Quantification of γH2AX band intensities from Fig.5A (n = 3). (**B**) Representative WB showing γH2AX in 20M and 54M VSMCs over-expressing FL-Runx2 and treated with H_2O_2 (3 hours). (**C** and **D**) Quantification of γH2AX band intensities relative to total H2AX (n = 3). (**E**) Quantification of comet assays shown in Fig. 5B (means from 3 independent experiments with n > 100 35F VSMCs. (**F**-**H**) Representative WB and quantification of γH2AX and pY142-H2AX in 35F VSMCs treated with H_2O_2 for 0-4 hours (n = 4). (**I**) Representative WB showing endogenous Runx2 in VSMCs expressing EGFP, shRunx2 or FL-Runx2 and with or without 3 hour H_2O_2 treatment. (**J**) WB showing elevated γH2AX and reduced pY142-H2AX in Runx2 KO mice (*Runx2*$^{\Delta SM}$) VSMCs. (**K**-**M**) Quantification of Runx2, γH2AX and pY142-H2AX in control (*Runx2*$^{f/f}$) and *Runx2*$^{\Delta SM}$ mice VSMCs before and after H_2O_2 (3 hour) treatment (n = 5). (**N**) End point readings from active Caspase 3 assay shown in Fig. 5F. (**O**) WB from co-immunoprecipitation assay using H2AX as bait protein to pull-down JNK in 35F, 20M and 54M VSMCs expressing either EGFP or FL-Runx2 and treated for 3 hours with etoposide.

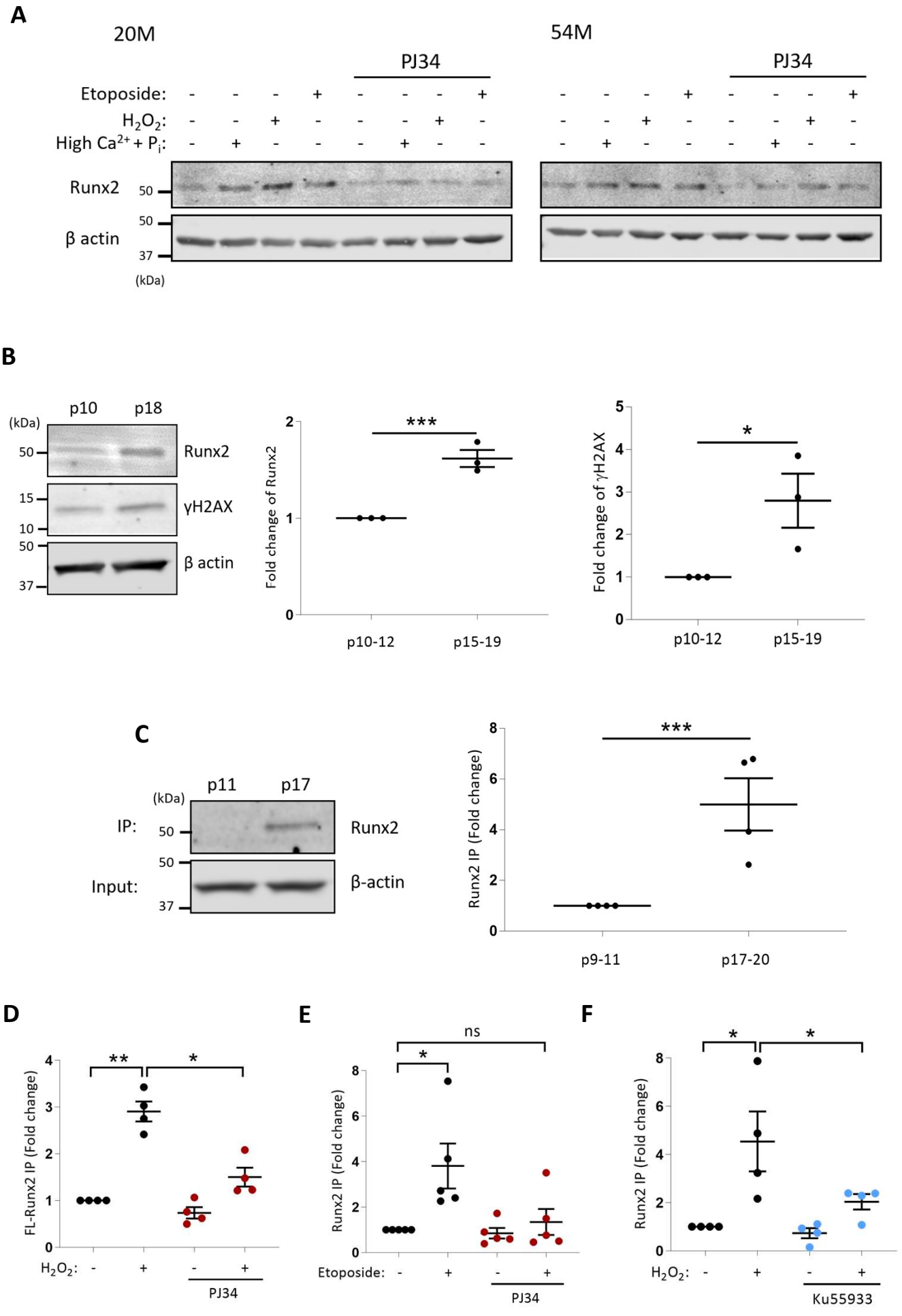
A
20M
54M
PJ34
Etoposide:
H_2O_2:
High Ca^{2+} + P_i:
Runx2
β actin
50
37
(kDa)
B
p10
p18
γH2AX
15
10
***
*
Fold change of Runx2
Fold change of γH2AX
p10-12
p15-19
C
p11
p17
IP:
Input:
β-actin
Runx2 IP (Fold change)
p9-11
p17-20
D
**
FL-Runx2 IP (Fold change)
E
ns
Etoposide:
F
Ku55933

Supplementary Fig. VI. **Runx2 is PARylated in response to genotoxic stress** (**A**) Representative WBs from BBPDAs investigating PARylation of Runx2 in 20M and 54M VSMCs cultured in calcifying media, H_2O_2 or etoposide and with or without PARP inhibitor PJ34 (10 days). β-actin is shown as lysate input control. (**B**) Representative WB and quantification of Runx2 and γH2AX in 35F VSMCs that have been aged *in vitro* by serial passaging (n = 3). (**C**) Representative WB and quantification of BBPDA comparing pull-down of Runx2 in early and late passage 35F VSMCs (n = 3). (**D**) Quantification of BBPDAs shown in Fig. 6D. (**E**) Quantification of BBPDAs shown in Fig. 6E. (**F**) Quantification of BBPDAs shown in Fig. 6F.

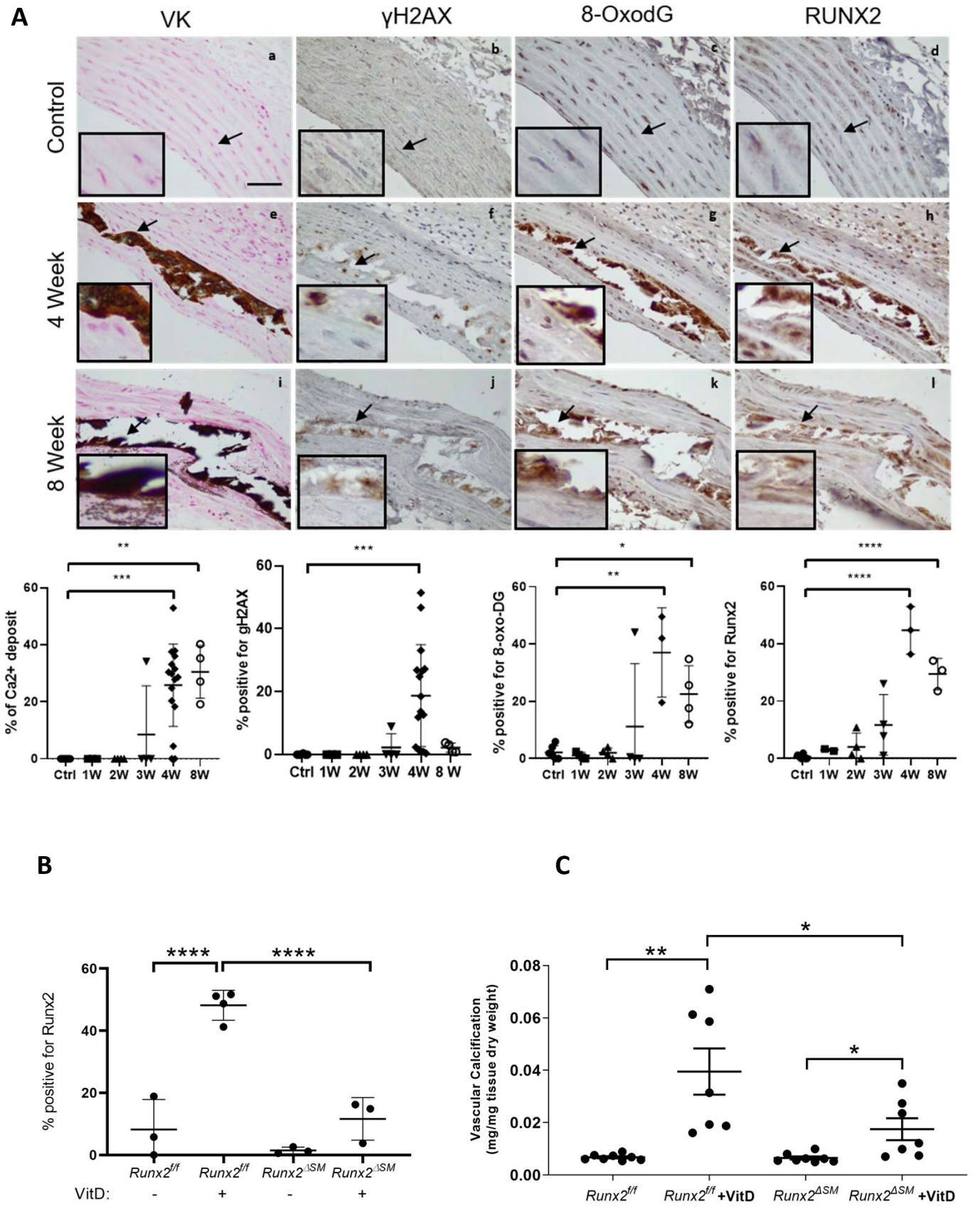
A
VK
γH2AX
8-OxodG
RUNX2
Control
4 Week
8 Week
a
b
c
d
e
f
g
h
i
j
k
l
% of Ca2+ deposit
% positive for gH2AX
% positive for 8-oxo-DG
% positive for Runx2
Ctrl 1W 2W 3W 4W 8W
Ctrl 1W 2W 3W 4W 8 W
B
% positive for Runx2
Runx2f/f
Runx2f/f
Runx2ΔSM
Runx2ΔSM
VitD: - + - +
C
Vascular Calcification (mg/mg tissue dry weight)
Runx2f/f
Runx2f/f +VitD
Runx2ΔSM
Runx2ΔSM +VitD

D

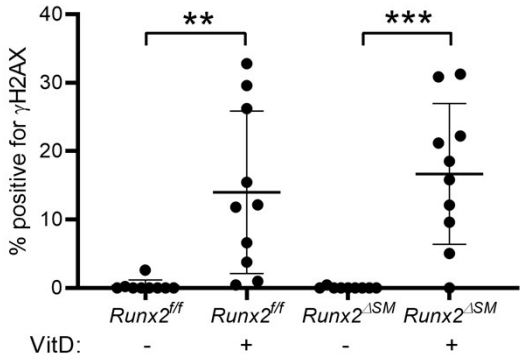
% positive for γH2AX
40
30
20
10
0
**
***
Runx2f/f
Runx2f/f
Runx2ΔSM
Runx2ΔSM
VitD:
-
+
-
+

E

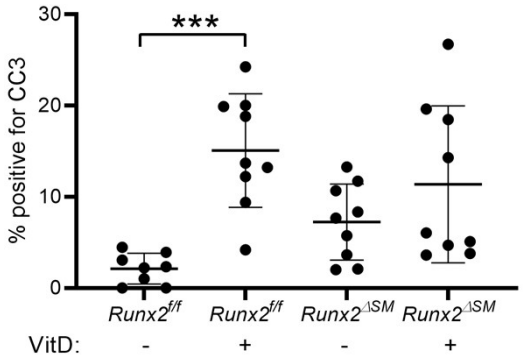
% positive for CC3
30
20
10
0
***
Runx2f/f
Runx2f/f
Runx2ΔSM
Runx2ΔSM
VitD:
-
+
-
+

F

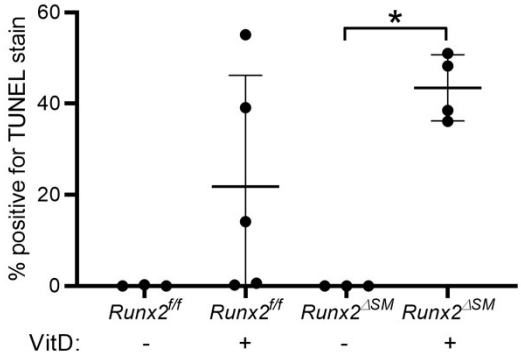
% positive for TUNEL stain
60
40
20
0
*
Runx2f/f
Runx2f/f
Runx2ΔSM
Runx2ΔSM
VitD:
-
+
-
+

G

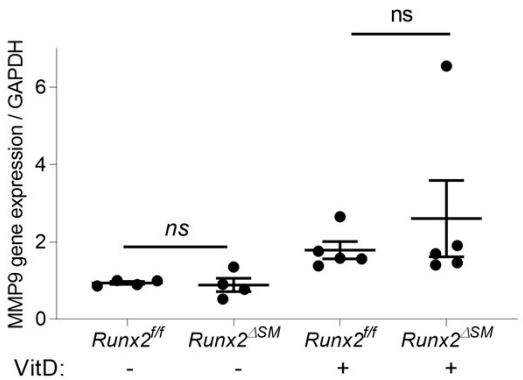
MMP9 gene expression / GAPDH
6
4
2
0
ns
ns
Runx2f/f
Runx2ΔSM
Runx2f/f
Runx2ΔSM
VitD:
-
-
+
+

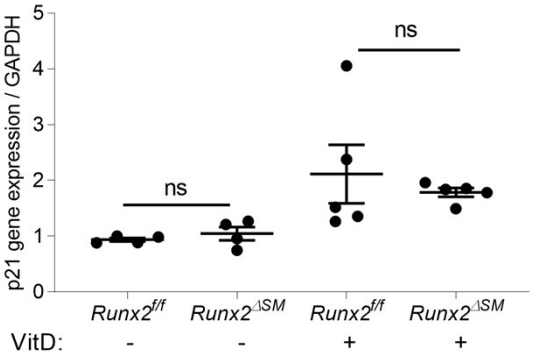
p21 gene expression / GAPDH
5
4
3
2
1
0
ns
ns
Runx2f/f
Runx2ΔSM
Runx2f/f
Runx2ΔSM
VitD:
-
-
+
+

Supplementary Fig. VII. **Runx2 localizes with γH2AX in calcified arteries, is essential for osteogenic gene expression and is PARylated in response to vitamin D treatment *in vivo.*** (**A**) Immunohistochemistry investigating arrangement of γH2AX, oxidised DNA lesions (8-OxodG) and Runx2 in calcified aortas taken from Wistar rats grown on a high Adenine diet for 4 or 8 weeks. VK = von Kossa staining. Black arrows indicate areas that have been enlarged. Scale bar is 2000 μm. Lower graphs show quantification of percentage of cells positive for γH2AX, calcification, 8-OxodG or Runx2. For controls n = 6, for 1W n = 3, for 2W n = 4, for 3W n = 4, for 4W n = minimum of 3 and for 8W n = minimum of 3. (**B**) IF quantification of Runx2 in and Runx2 KO aorta taken from *Runx2*$^{f/f}$ or *Runx2*$^{\Delta SM}$ mice treated with or without vitamin D (n = 3-4). (**C**) o-Cresolphthalein assay data comparing calcification between *Runx2*$^{f/f}$ and *Runx2*$^{\Delta SM}$ mice upon VitD treatment (n = minimum of 7). (**D** – **F**) Quantification of immunohistochemistry shown in Fig. 7B (n = minimum of 4). (**G**) RT-qPCR data showing *MMP9* (MMP9) and *CDKN1A* (p21) gene expression in the aorta of *Runx2*$^{f/f}$ or *Runx2*$^{\Delta SM}$ mice treated with or without vitamin D (n = 5).

S. Figure VIII

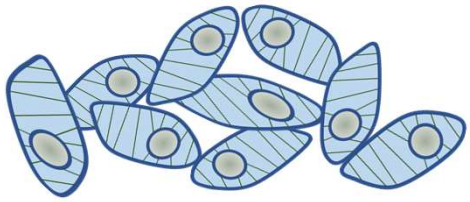

Healthy contractile VSMCs

Calcification stimulus

Elevated levels of DNA damage
ROS / ageing / senescenece

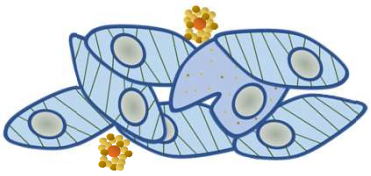

VSMC phenotype change
calcification initiated

ATM activation

PARP activity increases

Runx2 PARylation and accumulation

Increased expression of Runx2 osteogenic targets

Runx2 repression of DNA repair and activation of JNK dependent apoptosis

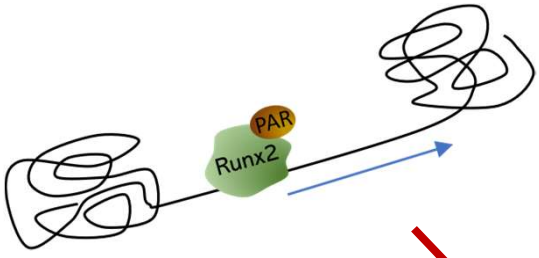

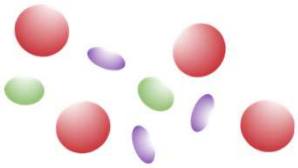

Increased Osteogenic differentiation

Cell death apoptotic body release

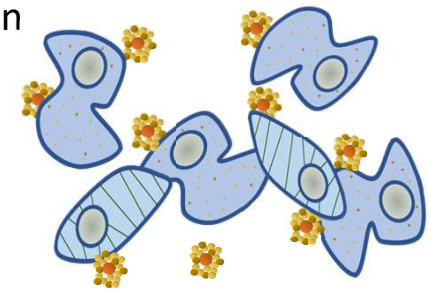

High levels of ECM calcification

Supplementary Fig. VIII **Schematic illustrating the role of Runx2 in augmenting VSMC calcification in the presence of DNA damage** VSMCs that have received a calcification stimulus will slowly calcify over time. However, in the presence of elevated DNA damage (for example in aged VSMCs or VSMCs exposed to genotoxic stressors) the DNA damage response is activated and ATM induces PARP mediated PARylation of Runx2 to cause its accumulation. This augments calcification in two ways: Firstly, we propose lower levels of DNA damage will result in expression of osteogenic Runx2 target genes due to increased occupancy of Runx2 at these promoter sites. Higher levels of DNA damage results in Runx2 promoting retention of pY142-H2AX and stimulation of JNK-mediated apoptosis which will promote vascular calcification through apoptotic body release.

Major Resources Table

In order to allow validation and replication of experiments, all essential research materials listed in the Methods should be included in the Major Resources Table below. Authors are encouraged to use public repositories for protocols, data, code, and other materials and provide persistent identifiers and/or links to repositories when available. Authors may add or delete rows as needed.

Animals (in vivo studies)

Species	Vendor or Source	Background Strain	Sex	Persistent ID / URL
Mouse	Taconic-Artemis	*C57BL/6*	M/F	Tac-Runx2tm2891.1Arte -Tg(CAG-Flpe)2Arte
Mouse	Professor Bennett lab, Cambridge.	*C57BL/6*	M/F	Tg(Tagln-cre)1Her/J
Rat	Charles River	Wistar rats	M	https://www.criver.com/products-services/find-model/wistar-igs-rat?region=3671

Genetically Modified Animals

	Species	Vendor or Source	Background Strain	Other Information	Persistent ID / URL
Parent	Mouse	Taconic-Artemis	*C57BL/6*		Tac-Runx2tm2891.1Arte -Tg(CAG-Flpe)2Arte
Parent	Mouse	Professor Bennett lab, Cambridge.	*C57BL/6*	https://www.jax.org/strain/004746	Tg(Tagln-cre)1Her/J

Antibodies

Target antigen	Vendor or Source	Catalog #	Working concentration	Lot # (preferred but not required)	Persistent ID / URL
Runx2	Santa Cruz Biotech	sc-10758	1 ug / ml		https://www.scbt.com/p/runx2-antibody-m-70
p53	Santa Cruz Biotech	sc-126	0.2 ug / ml		https://www.scbt.com/p/p53-antibody-do-1
DDDDK (Flag)	Sigma	F3165	0.5 ug / ml		https://www.sigmaaldrich.com/catalog/product/SIGMA/F3165?lang=en&region=GB
H2AX	Sigma	PLA0294	0.4 ug / ml		https://www.sigmaaldrich.com/catalog/product/sigma/pla0294?lang=en&region=GB
Beta actin	Sigma	AC-74	0.2 ug / ml		https://www.sigmaaldrich.com/catalog/product/sigma/a2228?lang=en&region=GB
8oxodG	JaICA	N45.1	1.5 ug / ml		https://www.jaica.com/e/products_dna_8ohdg_ab.html
DDDDK (Flag)	Abcam	ab1257	0.5 ug / ml		https://www.abcam.com/ddddk-tag-binds-to-flag-tag-sequence-antibody-ab1257.html
Ku70	Abcam	ab83501	1 ug / ml		https://www.abcam.com/ku70-antibody-ab83501.html
ERK1/2	Abcam	ab36991	0.5 ug /ml		https://www.abcam.com/erk1--erk2-antibody-9b3-ab36991.html

DOI [to be added]

pERK	Abcam	ab201015	0.8 ug /ml		https://www.abcam.com/erk1-phospho-t202--erk2-phospho-t185-antibody-epr19401-ab201015.html
pY142-H2AX	Abcam	ab94602	1 ug /ml		https://www.abcam.com/Histone-H2AX-phospho-Y142-antibody-ab94602.html?utm_source=biocompare&utm_medium=paid_referral&utm_campaign=editorial&utm_term=Primaries%20-%20Non-Recombinant_ab94602
αSMA	Abcam	ab7817	0.4 ug /ml		https://www.abcam.com/alpha-smooth-muscle-actin-antibody-1a4-ab7817.html
Runx2	Abcam	ab23981	1 ug /ml		https://www.abcam.com/runx2-antibody-ab23981.html
γH2AX	Cell signaling	2577	0.5 ug / ml		https://www.cellsignal.co.uk/products/primary-antibodies/phospho-histone-h2a-x-ser139-antibody/2577?Ntk=Products&Ntt=2577
Lamins AC	Cell signaling	2032	0.5 ug / ml		https://www.cellsignal.co.uk/products/primary-antibodies/lamin-a-c-antibody/2032?Ntk=Products&Ntt=2032
Chk2	Cell signaling	2662	1 ug / ml		https://www.cellsignal.co.uk/products/primary-antibodies/chk2-antibody/2662?Ntk=Products&Ntt=2662
pChk2 (T68)	Cell signaling	2197	1 ug /ml		https://www.cellsignal.co.uk/products/primary-antibodies/phospho-chk2-thr68-c13c1-rabbit-mab/2197?Ntk=Products&_=1601909014218&Ntt=2197&tahead=true
Cleaved caspase 3	Cell signaling	9661	0.6 ug /ml		https://www.cellsignal.co.uk/products/primary-antibodies/cleaved-caspase-3-asp175-antibody/9661?Ntk=Products&Ntt=9661
PAR	Novus Biologicals	4336-APC-050	2 ug/ ml		https://www.rndsystems.com/products/par-padpr-antibody_4336-apc-050

DNA/cDNA Clones

Clone Name	Sequence	Source / Repository	Persistent ID / URL

Cultured Cells

Name	Vendor or Source	Sex (F, M, or unknown)	Persistent ID / URL
04:35F:11A	Department of Medicine, Addenbrooke's Hospital, Cambridge	F	N/A
05:20M:18A	Department of Medicine, Addenbrooke's Hospital, Cambridge	M	N/A

DOI [to be added]

05:54M:20	Department of Medicine, Addenbrooke's Hospital, Cambridge	M	N/A
Mouse VSMC *Runx2*$^{f/f}$	This study	F	N/A
Mouse VSMC *Runx2*$^{\Delta SM}$	This study	F	N/A

Data & Code Availability

Description	Source / Repository	Persistent ID / URL

Other

Description	Source / Repository	Persistent ID / URL